



OPEN ACCESS

EDITED BY
Paola Marianelli,
University of Pisa, Italy

REVIEWED BY
Martin Mangler,
Durham University, United Kingdom
Károly Nemeth,
Massey University, New Zealand

*CORRESPONDENCE
Andres Sandoval-Velasquez,
andreslibardo.sandovalvelasquez@
community.unipa.it

SPECIALTY SECTION
This article was submitted to
Geochemistry,
a section of the journal
Frontiers in Earth Science

RECEIVED 20 June 2022
ACCEPTED 04 August 2022
PUBLISHED 07 September 2022

CITATION
Sandoval-Velasquez A, Rizzo AL,
Aiuppa A, Straub SM, Gomez-Tuena A
and Espinasa-Perena R (2022), The
heterogeneity of the Mexican
lithospheric mantle: Clues from noble
gas and CO₂ isotopes in fluid inclusions.
Front. Earth Sci. 10:973645.
doi: 10.3389/feart.2022.973645

COPYRIGHT
© 2022 Sandoval-Velasquez, Rizzo,
Aiuppa, Straub, Gomez-Tuena and
Espinasa-Perena. This is an open-
access article distributed under the
terms of the [Creative Commons
Attribution License \(CC BY\)](https://creativecommons.org/licenses/by/4.0/). The use,
distribution or reproduction in other
forums is permitted, provided the
original author(s) and the copyright
owner(s) are credited and that the
original publication in this journal is
cited, in accordance with accepted
academic practice. No use, distribution
or reproduction is permitted which does
not comply with these terms.

The heterogeneity of the Mexican lithospheric mantle: Clues from noble gas and CO₂ isotopes in fluid inclusions

Andres Sandoval-Velasquez^{1,2*}, Andrea Luca Rizzo^{1,3},
Alessandro Aiuppa², Susanne M. Straub⁴, Arturo Gomez-Tuena⁵
and Ramon Espinasa-Perena⁶

¹Istituto Nazionale di Geofisica e Vulcanologia, Sezione di Palermo, Palermo, Italy, ²DiSTeM, Università di Palermo, Via Archirafi, Palermo, Italy, ³Istituto Nazionale di Geofisica e Vulcanologia, Sezione di Milano, Milano, Italy, ⁴Lamont Doherty Earth Observatory at the Columbia Climate School, New York, NY, United States, ⁵Centro de Geociencias, Universidad Nacional Autónoma de México, Querétaro, México, ⁶Centro Nacional de Prevención de Desastres, Secretaría de Gobernación, Coyoacán, México

The abundance of mantle-derived rocks and lavas, in combination with its tectonic evolution, render Mexico a perfect laboratory to investigate the chemical and the isotopic heterogeneity of the lithospheric mantle. New data on the composition of noble gases and CO₂ in Mexican mantle xenoliths and lavas is reported. Our samples consist of six ultramafic nodules from the Durango Volcanic Field (DVF) and the San Quintin Volcanic Field (SQVF), monogenetic complexes belonging to the Mexican Basin and Range province; and four lavas from the Sierra Chichinautzin (SCN), a Quaternary monogenetic volcanic field located in the Mexican volcanic arc. Ne and Ar isotopes in fluid inclusions reveal mixing between atmospheric and MORB-like fluids (e.g., ⁴⁰Ar/³⁶Ar < 1,200). DVF and SQVF nodules record low ⁴⁰Ar/³⁶Ar and ⁴He/²⁰Ne that confirm the existence of recycled atmospheric-derived noble gases in the local mantle. The averages of the Rc/Ra ratios (³He/⁴He corrected for atmospheric contamination) measured in Mexican localities are within the MORB-like range: DVF = 8.39 ± 0.24 Ra, SQVF = 7.43 ± 0.19 Ra and SCN lavas = 7.15 ± 0.33 Ra (1σ). With the aim of assessing the isotopic variability of the Mexican lithospheric mantle, the above results were compared with similar data previously obtained from ultramafic nodules found in the Ventura Espiritu Santo Volcanic Field (VESVF), another Quaternary monogenetic volcanic complex belonging the Basin and Range. The higher ³He/⁴He ratios in DVF relative to those reported for the VESVF and the SQVF are explained as reflecting different ages of mantle refertilization, triggered by the retreating of the Farallon slab (~40 Ma ago) and associated delamination slab processes. We propose that the DVF mantle was refertilized more recently (<10 Ma ago) than the mantle beneath the SQVF and VESVF (~40–20 Ma ago). On the other hand, He-Ne-Ar compositions of SCN olivines share similarities with VESVF xenoliths,

Abbreviations: DVF, Durango Volcanic Field; SCLM, Subcontinental Lithospheric Mantle; SCN, Sierra Chichinautzin; SQVF, San Quintin Volcanic Field; TMVB, Trans-mexican Volcanic Belt; VESVF, Ventura Espiritu Santo Volcanic Field.

suggesting a relatively homogeneous lithospheric mantle in central Mexico. Finally, DVF and the SCN samples exhibit $\delta^{13}\text{C}$ values within the MORB range (comparable to other values previously reported in fluid inclusions and fumaroles from Popocatepetl, Colima–Ceboruco volcanoes). While we explain the MORB-like carbon signatures of the DVF samples as the result of the above-mentioned refertilization process, the SCN signatures likely reflect either (i) trapping of isotopically fractionated CO_2 derived from magmatic degassing or (ii) a mantle source unaffected by subduction-related crustal carbon recycling.

KEYWORDS

Basin and Range province, Trans-mexican Volcanic Belt, Mexican mantle xenoliths, arc lavas, fluid inclusions, noble gas isotopes, CO_2 isotopes, carbon recycling

1 Introduction

The Basin and Range is an extensional province in western North America stretching more than 2,500 km from the Idaho-Montana border (United States) to central Mexico (Figure 1A; Dickinson, 2002; Henry and Aranda-Gómez, 1992); it derives its name from the distinctive morphology, characterized by elongated horst alternating with alluvial basins. It is generally accepted that the tectonic evolution of Basin and Range started 30 Ma ago (during the middle-late Oligocene) as a result of the rollback and consumption of the horizontally dipping Farallon slab beneath the North American plate (Atwater, 1989; Sedlock, 2003; Ferrari et al., 2012). The tectonic changes that resulted included: (i) the migration of the volcanic arc from the N-NW-trending Sierra Madre Occidental to the present-day east-west TMVB (30–7 Ma), (ii) the transition from subduction to a transform margin (formation of the San Andreas fault system and the Mendocino and Rivera triple junctions ≈ 20 Ma ago), and (iii) regional extension that produced both the Gulf of California (≈ 10 –5 Ma ago) and the Basin and Range Province (Atwater, 1989; Severinghaus and Atwater, 1990; Sedlock et al., 1993; Ferrari et al., 1999, Ferrari et al., 2012; Nieto-Samaniego et al., 1999, Nieto-Samaniego et al., 2005; Bunge and Grand, 2000; Sedlock, 2003; Gómez-Tuena et al., 2007).

Like areas within the United States portion, the Mexican Basin and Range was accompanied by intraplate magmatism that generated several alkali basalt localities (Figure 1A; Basu, 1977; Gutmann, 1986; Aranda-Gómez and Ortega-Gutiérrez, 1987; Henry and Aranda-Gómez, 1992; Luhr and Aranda-Gomez, 1997). These volcanic fields represent a unique opportunity to study the characteristics of the local lithospheric mantle, since their deposits contain abundant mantle xenoliths (including both spinel peridotite varieties and pyroxenites; Basu, 1977; Gutmann, 1986; Aranda-Gómez and Ortega-Gutiérrez, 1987; Luhr et al., 1989; Pier et al., 1992; Luhr and Aranda-Gomez, 1997; Housh et al., 2010; Dávalos-Elizondo et al., 2016; Sandoval-Velasquez et al., 2021a); these (in view of the relatively rapid ascent of the host magma through the crust by short-lived monogenetic volcanic eruptions) are expected to retain the pristine

mineralogy and geochemical/isotopic characteristics of the mantle source (Pier et al., 1989; Luhr and Aranda-Gomez, 1997; Jackson, 1998; Pearson et al., 2014).

Thus, Mexico is a geodynamically complex area characterized by the coexistence of two distinct tectonic regimes. While the central and northwestern parts of the country are affected by continental extension and intraplate magmatism in the Basin and Range Province, southern Mexico has been dominated by subduction and continental arc magmatism during the last 17 Ma in the Trans-mexican Volcanic Belt (TMVB) (Figure 1; Henry and Aranda-Gómez, 1992; Ferrari et al., 1999; Ferrari et al., 2012; Aranda-Gómez et al., 2000; Dickinson, 2002; Sedlock, 2003; Gómez-Tuena et al., 2007).

In a previous work (Sandoval-Velasquez et al., 2021a), we investigated the isotopic composition of noble gases and CO_2 in fluid inclusions (FI) trapped in mantle xenoliths collected in the Ventura Espiritu Santo Volcanic Field (VESVF; Figure 1A). These results, integrated with information on petrography, mineral chemistry and fluid inclusion compositions from the same suite of samples, revealed a complex geological evolution, in which the central Mexican upper mantle was affected by metasomatism, refertilization and recycling of atmospheric noble gases and crustal carbon derived from the Farallon slab subduction.

Here, we extend our study to mantle xenoliths and lavas collected in other monogenetic volcanic fields belonging to the Mexican Basin and Range and TMVB provinces. In detail, we analyze the composition of FI in nodules from the Durango Volcanic Field (DVF), located in the Durango State (north of the VESVF; see Figure 1A), and from the San Quintin Volcanic Field (SQVF), located in Baja California peninsula. We also present the isotopic composition of FI trapped in olivine phenocrysts from lavas erupted in the Sierra Chichinautzin Volcanic Field (SCN), a Quaternary monogenetic volcanic system located in the TMVB (Figure 1B). The objective is to study the influence of the Farallon subduction in the composition and evolution of the Mexican lithospheric mantle in terms of volatiles. Our hypothesis points to the existence of a refertilized mantle whose Ar- CO_2 systematics have been modified by the introduction of air-derived noble gases

and crustal materials inherited from the extinct Farallon subduction. We rely on noble gas and CO₂ isotopes (coupled to petrological evidence), which are unique geodynamic tracers of the degassing history of the mantle, of the origin of Earth's volatiles, of the relationship between different mantle components, and of the nature and signature of metasomatic fluids in the mantle (Deines, 2002; Dunai and Porcelli, 2002; Gurenko et al., 2006; Dasgupta and Hirschmann, 2010; Day and Hilton, 2011; Day and Hilton, 2020; Correale et al., 2012, Correale et al., 2015; Rizzo et al., 2018; Li et al., 2019; Sandoval-Velasquez et al., 2021a; Sandoval-Velasquez et al., 2021b; Bekaert et al., 2021).

2 Tectonic and geological characteristics of the SQVF, DVF and the SCN

2.1 The Durango (DVF) and San Quintin (SQVF) volcanic fields

The DVF is located in the Mesa Central province, near the eastern border of the Sierra Madre Occidental (Figure 1A). This field covers more than 2000 km² and is composed of approximately 100 Pleistocene and Quaternary volcanic structures including maars, lava flows and cinder cones that represent at least 20 km³ of extruded magma (Albritton, 1958; Swanson, 1989; Aranda-Gómez et al., 1992; Luhr and Aranda-Gomez, 1997). In this work, we studied mantle xenoliths from the La Breña-El Jaguey maar complex, the most important xenolith locality in the DVF (Aranda-Gómez et al., 1992).

The La Breña -El Jaguey maar complex is located 45 km to the NW of Durango city (24° 25' 04.69"N and 104° 32' 04.86"W) and exhibits a peculiar morphology generated by the intersection of two different maars (Figure 2A): El Jaguey and La Breña. The El Jaguey is identified as a funnel-shaped maar with a diameter of 0.75 km, while La Breña is a nearly circular maar of 1.4 km in diameter (Swanson, 1989; Aranda-Gómez et al., 1992). These maars are believed to have formed from the interaction between an aquifer and a basanitic magma originated in the lithospheric mantle (Aranda-Gómez and Ortega-Gutiérrez, 1987; Henry and Aranda-Gómez, 1992; Luhr and Aranda-Gomez, 1997). No radiometric ages have been reported for these events, however, it is believed that the maar-related eruptions are Quaternary (Swanson, 1989; Aranda-Gómez et al., 1992).

Unlike the VESVF (see Sandoval-Velasquez et al., 2021a) and the DVF, the SQVF is situated in northwestern Mexico, in the Baja California state near the Mexico-USA border (Figure 1). The SQVF is the only mantle xenolith-bearing alkaline basalt complex identified in the Baja California Peninsula, and formed as consequence of opening of the Gulf of California (at 3.5 Ma) after subduction of the Farallon plate terminated at 12 Ma (Aranda-Gómez and Ortega-Gutiérrez, 1987; Luhr et al., 1995a; Luhr and Aranda-Gomez, 1997; Sedlock, 2003). Geochemical signatures of SQVF magmas, and the presence of mantle xenoliths, support similarity with deformation

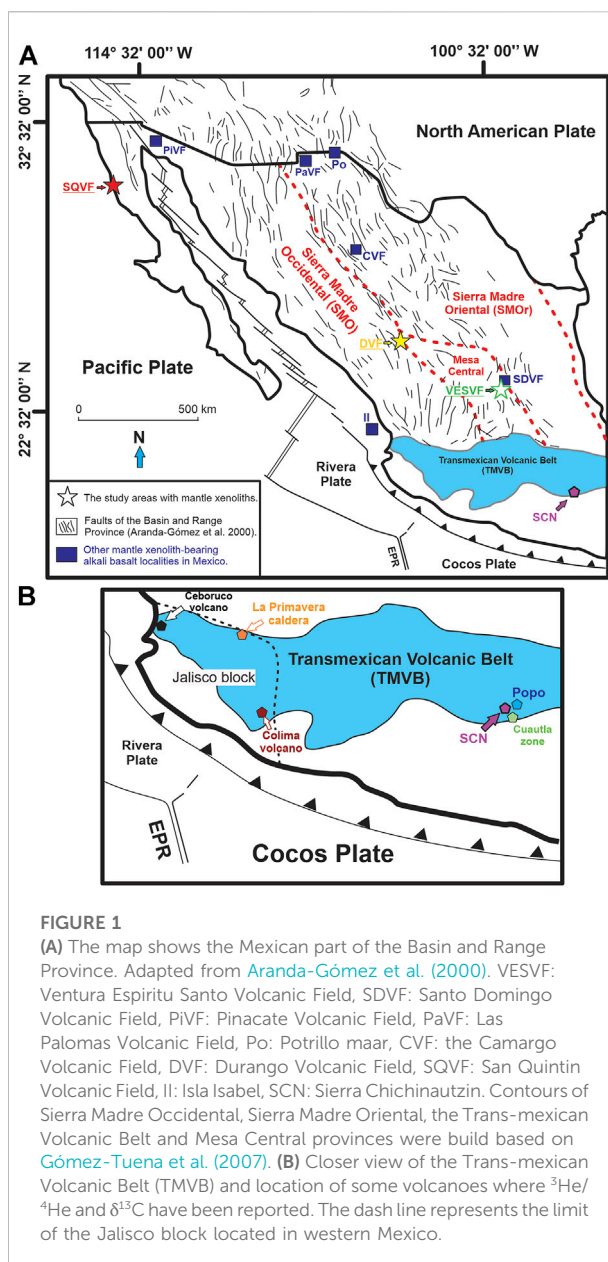


FIGURE 1

(A) The map shows the Mexican part of the Basin and Range Province. Adapted from Aranda-Gómez et al. (2000). VESVF: Ventura Espiritu Santo Volcanic Field, SDVF: Santo Domingo Volcanic Field, PIVF: Pinacate Volcanic Field, PaVF: Las Palomas Volcanic Field, Po: Potrillo maar, CVP: the Camargo Volcanic Field, DVF: Durango Volcanic Field, SQVF: San Quintin Volcanic Field, Il: Isla Isabel, SCN: Sierra Chichinautzin. Contours of Sierra Madre Occidental, Sierra Madre Oriental, the Trans-mexican Volcanic Belt and Mesa Central provinces were built based on Gómez-Tuena et al. (2007). (B) Closer view of the Trans-mexican Volcanic Belt (TMVB) and location of some volcanoes where ³He/⁴He and δ¹³C have been reported. The dash line represents the limit of the Jalisco block located in western Mexico.

and tectonic style of the Basin and Range extensional province (Aranda-Gómez and Ortega-Gutiérrez, 1987; Luhr et al., 1989; Pier et al., 1989; Luhr et al., 1995a).

Volcanic activity in the SQVF started during the Pleistocene and continued through the Holocene (Luhr et al., 1995a; Luhr and Aranda-Gomez, 1997); some peperites and pillow lavas have also been identified in the volcanic field suggesting that the SQVF initiated as a group of subaqueous volcanoes that later emerged (Surtseyan-style activity; Németh and Kósik, 2020). The SQVF consists of 10 different volcanic complexes; each complex is characterized by a well-preserved scoria cone, several eruptive vents and lava flows (Luhr et al., 1995a; Luhr and Aranda-

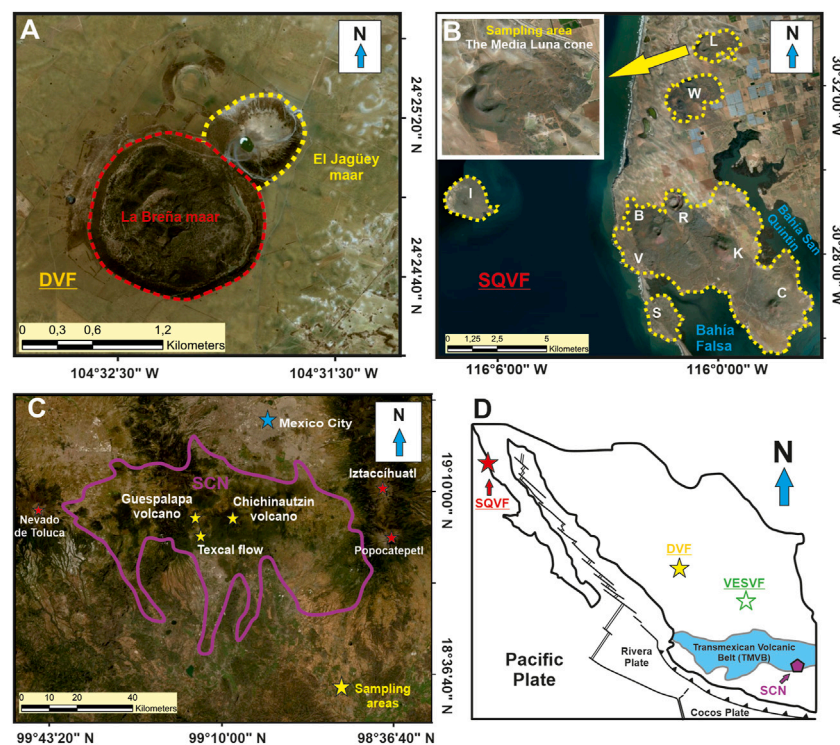


FIGURE 2

(A) Image from Google Earth (23 June 2021) showing La Breña-El Jagüey maar complex. (B) Image from Google Earth (23 June 2021) showing the San Quintin Volcanic Field (SQVF) and sampling area. Media Luna (L), Woodford (W), Basu (B), Riveroll (R), Kenton (K), Picacho Vizcaíno (P), Sudoeste (S), Ceniza (C), Monte Mazo (M) and Isla San Martín (I). (C) Image from Google Earth (23 June 2021) showing the Sierra Chichinautzin (SCN) and sampling areas. (D) Mexico overview map including the SQVF, DVF, VESVF, and SCN localities.

Gomez, 1997). These volcanic complexes are (Figures 2B,D): the Media Luna (L), Woodford (W), Basu (B), Riveroll (R), Kenton (K), Picacho Vizcaíno (P), Sudoeste (S), Ceniza (C), Monte Mazo (M) and Isla San Martín (I). Mantle xenoliths analyzed in this work come from the Media Luna cone.

2.2 The Sierra Chichinautzin (SCN)

The SCN is a Quaternary monogenetic volcanic field located along the Trans-Mexican Volcanic Belt (TMVB) front, and in between two Quaternary stratovolcanoes: Popocatepetl and Nevado de Toluca (Figures 1B, 2C; Márquez et al., 1999a; Márquez et al., 1999b; Schaaf et al., 2005; Meriggi et al., 2008). The SCN has been active over the last 40 ka producing more than 200 volcanic monogenetic structures (including several scoria cones, lava flows, lava domes, shield volcanoes and hydromagmatic craters) and approximately 470 km³ of extruded magma (Márquez et al., 1999a, Márquez et al., 1999b; Schaaf et al., 2005; Meriggi et al., 2008). Erupted rocks include basalts, basaltic andesites, andesites and dacites (Márquez et al., 1999b; Meriggi et al., 2008). The origin of the SCN is still controversial and different hypotheses have been set out in the literature. One model suggests

that the calc-alkaline affinity and the LILE-Pb enrichments (identified in evolved rocks) are the result of partial melting of a subduction-related metasomatized mantle wedge (Meriggi et al., 2008; Straub et al., 2011; Straub et al., 2013; Straub et al., 2014; Straub et al., 2015). Other studies (Márquez et al., 1999a; Márquez et al., 1999b) argue that the above hypothesis is inconsistent with the presence of OIB-type (high-Nb) mafic rocks in the SCN; therefore, they propose an extensional origin for the monogenetic SCN. These authors suggest that the OIB geochemical affinity of the SCN basalts is a result of partial melting of a mantle not affected by subduction, and that the calc-alkaline affinity of the most evolved rocks derives from magma mixing between basaltic magmas and crustal-derived felsic magmas (Márquez et al., 1999a; Márquez et al., 1999b).

3 Petrological background of mantle xenoliths and lavas

According to Luhr and Aranda-Gomez (1997), mantle xenoliths from the DVF are dominated by coarse-tabular and protogranular textures and are characterized by the presence of clusters of spinel (Sp), orthopyroxene (Opx) and clinopyroxene (Cpx) (possibly originated from the decompressive reaction of

TABLE 1 Coordinates for sampling areas.

Sample	Locality	Type	Latitude	Longitude
SQVF xenolith	Media luna cone	Ultramafic xenolith	30°32' 52"N	116°00'16"W
DVF xenoliths	La breña-El jaguey maar complex	Ultramafic xenoliths	24°25'00"N	104°32' 10"W
CH09-1 and CH09-9	Guespalapa volcano	lava	19°05'26"N	99°10'38"W
MCH-06-5	Chichinautzin volcano	lava	19°06'02"N	99°04'40"W
CH-05-16	Texcal flow	lava	19°04'49"N	99°11'52"W

olivine and garnet). Olivine (Ol) and Opx crystals from DVF samples usually have diameters >2 mm, while Cpx and Sp exhibit variable diameters between 1–2 mm. SQVF xenoliths generally show strongly deformed fabrics with a bimodal grain-size distribution (porphyroclastic texture); samples may exhibit porphyroclasts of Ol and Opx with diameters greater than 5 mm surrounded by recrystallized neoblasts, with sizes <1 mm, of Ol, Opx, Cpx, and Sp. A common characteristic of DVF and SQVF xenoliths is the presence of interstitial glass veins and spongy rims in Cpx. Interstitial glasses have elevated SiO₂ (54–57 wt%), Al₂O₃ (18–21 wt%), Na₂O (2.5–6.1 wt%), K₂O (1.5–5.7 wt%), P₂O₅ (0.06–0.81 wt%), and are MgO-depleted (2.5–3.6 wt%). Spongy rims in Cpx show elevated Mg#, are enriched in CaO and depleted in Al₂O₃ and Na₂O, as observed in VESVF xenoliths. Luhr and Aranda-Gomez (1997) proposed that both glasses and spongy rims may be the result of either of two different processes: 1) partial melting or 2) the infiltration of volatile-rich melts reacting with the lithospheric mantle. The above authors also report pressures of 17.7 ± 1.7 kbar and fO₂ values (ΔFMQ; where FMQ is the fayalite-magnetite-quartz buffer) of -0.2 ± 0.3 for the DVF xenoliths and pressures around 10.7 ± 2.5 kbar and fO₂ (ΔFMQ) of 0.0 ± 0.2 for the SQVF samples. Luhr and Aranda-Gomez (1997) argued that the systemic increase of mantle xenolith's oxygen fugacity from DVF to SQVF derives from subduction-related oxidation of the lithospheric mantle, due to the release of fluids from the subducted Farallon slab beneath the North American plate.

Petrological and isotopic results (Sr-Pb-Nd-He) for SCN lavas have proven that both andesites and basalts directly derive from the local mantle. According to Straub et al. (2008), Straub et al. (2011), these rocks show common geochemical characteristics that suggest a similar genetic mechanism. Andesites and basalts are consistently enriched in Ni and MgO (with melt Mg#~ 70), they show similar ratios of trace elements (e.g., Sr/Y and Gd/Yb), and contain Ni-rich olivines with MORB-like ³He/⁴He ratios. Schaaf et al. (2005) and Straub et al. (2011) propose that the occurrence of high-Mg calc-alkaline and alkaline primitive magmas in the SCN suggest that magmas accumulate in small and short-lived magmatic systems with negligible crustal contamination. Moreover, using tracers such as ³He/⁴He and δ¹⁸O, Straub et al. (2022) demonstrated that olivine phenocrysts grow into mantle melts not contaminated by crustal materials. The opposite occurs for Popocatepetl lavas since generally

reflect long crustal residence in shallow magma chambers and assimilation of Cretaceous limestones (Schaaf et al., 2005; Witter et al., 2005; Mangler et al., 2019).

Straub et al. (2008), Straub et al. (2011) argue that both andesites and basalts originated from partial melting of peridotites and coexisting silica-deficient and quartz-normative pyroxenites (located below the Moho) that were produced by the infiltration of silicic slab melts in the local mantle. After melting, a broad spectrum of high-Mg# basaltic, andesitic and dacitic melts were generated; during their ascent through the crust, these eventually undergo differentiation by fractional crystallization and recharge melt mixing in the overlying crust (just before the eruption), leading to Mg#<65 lavas.

4 Samples and methods

Six peridotites (1 lherzolite from the SQVF and 4 lherzolites and 1 harzburgite from the DVF) and 4 lava samples (from the SCN) were analyzed in this study. Peridotites from the SQVF and the DVF were provided by the Department of Mineral Sciences of the Smithsonian Institution. SQVF sample was originally collected in the Media Luna cone, while DVF samples come from the La Breña -El Jaguey maar complex. SCN lavas are two calc-alkaline basaltic andesites (samples CH09-1 and CH09-9) and two high-Nb arc basalts (samples CH05-16 and MCH06-5). Sample CH05-16 was collected from the Texcal Flow, samples CH09-1 and CH09-9 were collected in the Guespalapa volcano, while sample MCH-06-5 was obtained from the Chichinautzin volcano (see Table 1 and Figure 2 for coordinates).

Mantle xenoliths and lavas were crushed for noble gas and CO₂ isotopic determinations following the same methods and analytical procedures described in Rizzo et al. (2018), Rizzo et al. (2021), Sandoval-Velasquez et al. (2021a), and Sandoval-Velasquez et al. (2021b). After crushing, samples were sieved with the aim of hand-picking crystals (with diameters >0.25 mm) of Ol, Opx, and Cpx from mantle xenoliths and only Ol crystals from lavas. Aliquots of crystals (weights of 0.5–2 g) were properly cleaned ultrasonically, accurately weighed and loaded into an ultra-high-vacuum (UHV) crusher for noble gas analyses. FI were released by single-step crushing at about 200 bar and room temperature (21°C). The gas mixture was purified in a stainless-

TABLE 2 Fluid inclusion compositions from DVF–SQVF mantle xenoliths and SCN olivine-related lavas. Concentrations of noble gases isotopes and CO₂ are reported in mol/g.

Sample ID	Phase	Locality	Weight (g)	³ He	⁴ He	²⁰ Ne	²¹ Ne	²² Ne	CO ₂ ^a	⁴⁰ Ar	⁴⁰ Ar*	⁴ He/ ²⁰ Ne	X ^c	⁴ He/ ⁴⁰ Ar*
NMNH-116610 18	Ol	DVF	1.08003	2.87E-18	2.47E-13	2.10E-15	6.13E-18	2.10E-16	1.75E-09	1.72E-13	9.82E-14	117.6	369.9	2.52
NMNH-116610 18	Opx	DVF	1.03656	7.41E-18	7.00E-13	3.41E-15	9.37E-18	3.55E-16	3.04E-09	9.52E-13	4.93E-13	205.2	645.1	1.42
NMNH-116610 18	Cpx	DVF	0.69300	1.76E-18	1.95E-13	2.56E-15	6.87E-18	2.74E-16	1.59E-08	1.24E-12	8.43E-13	76.2	239.6	0.23
NMNH-116610 20	Ol	DVF	1.03079	5.68E-18	5.00E-13	1.52E-14	4.57E-17	1.57E-15	5.28E-09	5.62E-12	3.94E-13	32.8	103.3	1.27
NMNH-116610 20	Opx	DVF	1.39776	8.94E-18	9.15E-13	4.42E-14	1.30E-16	4.47E-15	9.87E-09	9.48E-12	n.a	20.7	65.1	n.a
NMNH-116610 20	Cpx	DVF	0.41756	1.03E-17	1.13E-12	1.67E-14	4.85E-17	1.69E-15	1.56E-08	6.63E-12	1.84E-12	67.7	213.0	0.61
NMNH-116610 27	Ol	SQVF	1.07264	5.69E-19	5.51E-14	1.59E-15	4.63E-18	1.60E-16	2.36E-09	3.08E-13	3.88E-14	34.8	109.3	1.42
NMNH-116610 27	Opx	SQVF	1.11606	2.08E-19	2.74E-14	9.98E-16	2.80E-18	1.02E-16	2.34E-09	1.30E-13	5.36E-14	27.5	86.5	0.51
NMNH-116610 27	Cpx	SQVF	0.55603	1.39E-19	1.96E-14	1.18E-15	5.26E-18	4.36E-16	8.33E-11	4.23E-14	3.02E-14	16.5	51.9	0.65
NMNH-117214 36	Ol	DVF	1.07046	1.15E-18	1.01E-13	3.14E-15	9.13E-18	3.22E-16	8.81E-09	8.88E-13	1.08E-13	32.2	101.1	0.93
NMNH-117214 36	Opx	DVF	1.13955	3.50E-18	3.24E-13	3.51E-15	1.02E-17	3.65E-16	3.10E-09	9.20E-13	2.26E-13	92.3	290.3	1.44
NMNH-117214 36	Cpx	DVF	0.57902	6.51E-18	6.45E-13	3.23E-14	9.66E-17	3.29E-15	1.44E-08	1.23E-11	1.35E-12	20.0	62.9	0.48
NMNH-117214 37	Ol	DVF	1.07363	5.29E-19	4.80E-14	6.17E-16	1.94E-18	6.26E-17	8.83E-10	1.37E-13	4.61E-14	77.8	244.7	1.04
NMNH-117214 37	Opx	DVF	1.10433	1.78E-18	1.67E-13	2.02E-15	7.49E-18	3.90E-16	2.14E-09	3.44E-13	1.70E-13	82.5	259.5	0.98
NMNH-117214 37	Cpx	DVF	0.52719	5.40E-18	4.63E-13	4.04E-14	1.19E-16	4.13E-15	1.54E-08	1.37E-11	1.32E-12	11.5	36.2	0.35
NMNH-117214 39	Ol	DVF	1.01815	1.28E-18	1.16E-13	3.38E-15	9.90E-18	3.45E-16	2.02E-09	6.35E-13	3.35E-13	34.5	108.3	0.35
NMNH-117214 39	Opx	DVF	1.01739	1.65E-18	1.74E-13	1.10E-14	3.26E-17	1.13E-15	1.39E-08	4.38E-12	1.52E-12	15.8	49.8	0.11
NMNH-117214 39	Cpx	DVF	0.50192	2.72E-18	2.95E-13	1.23E-14	3.60E-17	1.27E-15	1.21E-08	4.79E-12	2.17E-12	24.0	75.5	0.14
CH09-1	Ol	SCN	0.48322	2.38E-16	2.46E-11	9.08E-15	2.77E-17	9.33E-16	7.17E-07	4.89E-12	2.82E-12	2,704.2	8,503.8	8.71
CH09-9	Ol	SCN	0.51047	3.94E-16	3.99E-11	1.39E-14	4.26E-17	1.44E-15	1.29E-06	1.24E-11	7.21E-12	2,879.6	9,055.5	5.54
CH05-16	Ol	SCN	0.48009	7.43E-17	7.26E-12	1.36E-14	4.02E-17	1.37E-15	1.60E-07	2.68E-12	1.97E-12	535.8	1,684.8	3.68
MCH06-5	Ol	SCN	0.71327	9.98E-18	1.00E-12	1.90E-14	5.50E-17	1.90E-15	1.17E-08	8.79E-13	2.51E-13	52.8	166.1	3.98

Sample	Phase	R/Ra	Rc/Ra	error +/- (1σ)	⁴⁰ Ar/ ³⁶ Ar	error +/- (1σ)	²⁰ Ne/ ²² Ne	error +/- (1σ)	²¹ Ne/ ²² Ne	error +/- (1σ)	CO ₂ / ³ He	³ He/ ³⁶ Ar	CO ₂ / ³ He	CO ₂ ^b	δ ¹³ C
NMNH-116610 18	Ol	8.33	8.35	0.14	690.34	4.26	10.02	0.04	0.0293	0.0009	6.11E+08	0.0115	n.a	n.a	n.a
NMNH-116610 18	Opx	7.60	7.62	0.16	612.69	0.81	9.94	0.05	0.0273	0.0006	4.10E+08	0.0015	n.a	n.a	n.a
NMNH-116610 18	Cpx	6.46	6.48	0.20	926.66	1.82	9.92	0.08	0.0267	0.0011	4.29E+09	0.0006	n.a	n.a	n.a

(Continued on following page)

TABLE 2 (Continued) Fluid inclusion compositions from DVF—SQVF mantle xenoliths and SCN olivine-related lavas. Concentrations of noble gases isotopes and CO₂ are reported in mol/g.

Sample	Phase	R/ Ra	Rc/ Ra	error +/- (1σ)	⁴⁰ Ar/ ³⁶ Ar	error +/- (1σ)	²⁰ Ne/ ²² Ne	error +/- (1σ)	²¹ Ne/ ²² Ne	error +/- (1σ)	CO ₂ / ³ He	³ He/ ³⁶ Ar	CO ₂ / ³ He	CO ₂ ^b	δ ¹³ C
NMNH-116610 20	Ol	8.10	8.17	0.10	317.79	0.22	9.68	0.01	0.0291	0.0002	9.30E+08	0.0003	n.a	n.a	n.a
NMNH-116610 20	Opx	6.93	7.03	0.14	278.99	0.75	9.94	0.01	0.0294	0.0002	1.10E+09	0.0008	n.a	n.a	n.a
NMNH-116610 20	Cpx	6.53	6.56	0.19	409.01	0.28	9.95	0.02	0.0290	0.0003	1.52E+09	0.0034	n.a	n.a	n.a
NMNH-116610 27	Ol	7.37	7.43	0.19	338.17	0.53	9.91	0.05	0.0290	0.0008	4.14E+09	0.0006	n.a	n.a	n.a
NMNH-116610 27	Opx	5.39	5.44	0.25	503.73	2.24	9.91	0.12	0.0279	0.0019	1.13E+10	0.0002	n.a	n.a	n.a
NMNH-116610 27	Cpx	5.02	5.10	0.52	1,031.96	17.06	12.57	0.09	0.0562	0.0024	6.00E+08	0.0002	n.a	n.a	n.a
NMNH-117214 36	Ol	8.13	8.20	0.16	336.63	0.17	9.75	0.04	0.0284	0.0006	3.31E+09	0.0004	n.a	n.a	n.a
NMNH-117214 36	Opx	7.74	7.77	0.18	391.54	0.33	9.91	0.04	0.0289	0.0006	8.87E+08	0.0030	n.a	n.a	n.a
NMNH-117214 36	Cpx	7.16	7.27	0.14	332.06	1.17	9.80	0.01	0.0294	0.0002	2.21E+09	0.0001	n.a	n.a	n.a
NMNH-117214 37	Ol	7.90	7.93	0.24	445.15	1.88	9.85	0.09	0.0311	0.0020	1.67E+09	0.0017	n.a	n.a	n.a
NMNH-117214 37	Opx	7.65	7.68	0.18	585.04	3.78	10.76	0.04	0.0400	0.0007	1.20E+09	0.0003	n.a	n.a	n.a
NMNH-117214 37	Cpx	8.18	8.40	0.16	327.04	0.98	9.84	0.01	0.0291	0.0002	2.85E+09	0.0003	n.a	n.a	n.a
NMNH-117214 39	Ol	7.84	7.90	0.14	626.51	0.98	9.79	0.03	0.0287	0.0006	1.58E+09	0.0013	n.a	n.a	n.a
NMNH-117214 39	Opx	6.68	6.80	0.16	452.62	0.30	9.88	0.02	0.0293	0.0003	8.44E+09	0.0048	3.06E+09	1.09E-08	-5.43
NMNH-117214 39	Cpx	6.56	6.64	0.17	540.20	0.38	9.90	0.02	0.0291	0.0003	4.43E+09	0.0013	1.55E+09	6.55E-09	-3.80
CH09-1	Ol	6.99	6.99	0.068	697.30	0.07	9.74	0.03	0.0273	0.0005	4.10E+08	0.0340	4.08E+09	9.74E-07	-6.13
CH09-9	Ol	7.10	7.10	0.065	706.09	0.76	9.65	0.02	0.0267	0.0004	4.29E+09	0.0224	3.61E+09	1.42E-06	-6.31
CH05-16	Ol	7.36	7.36	0.096	1,117.31	0.10	9.93	0.02	0.0291	0.0003	9.30E+08	0.0310	3.88E+09	2.88E-07	-5.00
MCH06-5	Ol	7.13	7.17	0.103	414.01	0.08	10.06	0.01	0.0294	0.0002	1.10E+09	0.0047	n.a	n.a	n.a

^aFirst estimation of CO₂ during noble gases analysis.

^bCO₂ measured from glass line. Estimated errors for ³He, ⁴He, ²⁰Ne, ²¹Ne, ²²Ne, ⁴⁰Ar, ³⁶Ar, and CO₂ are <5%, <0.03%, <7%, <5%, <0.7%, <0.07%, <0.1%, and <5%, respectively.

^cX values were calculated following the equations described by [Harðardóttir et al. \(2018\)](#).

steel ultra-high-vacuum preparation line to remove all gas species (N₂, H₂, H₂O, and CO₂) except noble gases. The first estimation of CO₂ concentrations in FI was performed for each sample (manometric determination). He and Ne isotopes were analyzed using two different split-flight-tube mass spectrometers (Helix SFT-Thermo), while Ar isotopes were analyzed by a multi-collector mass spectrometer (Argus, GVI); typical blanks for He, Ne, and Ar were <10⁻¹⁵, <10⁻¹⁶, and <10⁻¹⁴ mol, respectively.

The measured ³He/⁴He ratios were corrected for atmospheric contamination based on the measured ⁴He/²⁰Ne ratio and the values are expressed as R_c/R_a:

$$R_c/R_a = ((R_M/R_a)(He/Ne)_M - (He/Ne)_A) / ((He/Ne)_M - (He/Ne)_A) \quad (1)$$

where R_M/R_a and (He/Ne)_M are the measured values and (He/Ne)_A refers to the atmospheric value (0.318; [Ozima and Podosek, 2002](#)). ⁴⁰Ar and ⁴He/²⁰Ne values were also corrected for atmospheric contamination:

$${}^{40}\text{Ar}^* = {}^{40}\text{Ar}_{\text{sample}} - ({}^{36}\text{Ar}_{\text{sample}} \cdot ({}^{40}\text{Ar}/{}^{36}\text{Ar})_{\text{air}}) \quad (2)$$

$$X(\text{air} - \text{normalized } {}^4\text{He}/{}^{20}\text{Ne}_{\text{mantle and crustal samples}}) = \frac{({}^4\text{He}/{}^{20}\text{Ne})_{\text{measured}}}{({}^4\text{He}/{}^{20}\text{Ne})_{\text{air}}} \quad (3)$$

$$X(\text{air} - \text{normalized } {}^4\text{He}/{}^{20}\text{Ne}_{\text{fluid samples}}) = \frac{({}^4\text{He}/{}^{20}\text{Ne})_{\text{measured}}}{({}^4\text{He}/{}^{20}\text{Ne})_{\text{air}}} \cdot \frac{\beta_{\text{Ne}}}{\beta_{\text{He}}} \quad (4)$$

where ${}^{40}\text{Ar}^*$ is the corrected ${}^{40}\text{Ar}$, ${}^{40}\text{Ar}/{}^{36}\text{Ar}_{\text{air}} = 298.56$ (Lee et al., 2006), β_{Ne} and β_{He} are the Bunsen solubility coefficients for Ne and He, respectively (IUPAC, 1979; Harðardóttir et al., 2018). Abundances of ${}^{20}\text{Ne}$, ${}^{21}\text{Ne}$, ${}^{22}\text{Ne}$, ${}^{36}\text{Ar}$, and ${}^{38}\text{Ar}$ are reported. Analytical uncertainties (1σ) for ${}^3\text{He}/{}^4\text{He}$, ${}^{20}\text{Ne}/{}^{22}\text{Ne}$, ${}^{21}\text{Ne}/{}^{22}\text{Ne}$ and ${}^{40}\text{Ar}/{}^{36}\text{Ar}$ ratios are $<4.4\%$, $<1.0\%$, $<6.8\%$ and $<2.2\%$, respectively. The ${}^{20}\text{Ne}/{}^{22}\text{Ne}$ and ${}^{21}\text{Ne}/{}^{22}\text{Ne}$ ratios were properly corrected (please see Rizzo et al., 2018 and Sandoval-Velasquez et al., 2021a).

The aliquots with the highest concentrations of CO_2 ($n = 6$) were selected to determine the carbon isotopic composition of FI (${}^{13}\text{C}/{}^{12}\text{C}$). Samples were properly cleaned, weighed and loaded in a crusher system consisting of a stainless-steel sample holder, a hydraulic crusher a glass sampler to freeze CO_2 , and a pump to ensure the vacuum inside the system. The gas mixture trapped in the FI was released and purified in a glass line equipped with a 626B Baratron[®] Absolute Capacitance Manometer MKS (measuring range 10^{-3} – 10^{-4} mbar), for the purification procedure and quantification of CO_2 concentration (mol/g). The ${}^{13}\text{C}/{}^{12}\text{C}$ ratios were measured using a Thermo (Finnigan) Delta Plus XP CF-IRMS connected to a Trace GC gas chromatograph and a Thermo (Finnigan) GC/C III interface. Results are expressed in parts per thousand (‰; relative to the V-PDB international standard) using the delta notation ($\delta^{13}\text{C}$). The analytical error estimated as $1\sigma < 0.6\%$. Detailed information about the methodology can be found in Gennaro et al. (2017), Rizzo et al. (2018) and Sandoval-Velasquez et al. (2021b).

5 Results

The composition of FI trapped in mantle xenoliths and lavas is reported in Table 2 and Figure 3. Errors are reported as 1σ uncertainties. CO_2 is the dominant volatile species in the FI; its concentration ranges from 8.33×10^{-11} to 1.54×10^{-8} mol/g. Samples from the DVF generally exhibit higher gas (${}^4\text{He}$, ${}^{40}\text{Ar}^*$, and CO_2) concentrations than those from SQVF. In general, ${}^3\text{He}$ and ${}^4\text{He}$ concentrations vary from 1.38×10^{-19} to 1.32×10^{-17} mol/g and 1.96×10^{-14} to 1.51×10^{-12} mol/g, respectively. ${}^{40}\text{Ar}^*$ (Ar content corrected for the atmospheric contamination) ranges from 3.02×10^{-14} to 2.17×10^{-12} mol/g. Rc/Ra values (${}^3\text{He}/{}^4\text{He}$ corrected for the atmospheric contamination) vary from 5.10 to 8.40 with the lowest values being observed in pyroxenes from SQVF (Figure 4). On average, the Rc/Ra ratios obtained in DVF xenoliths are higher than the

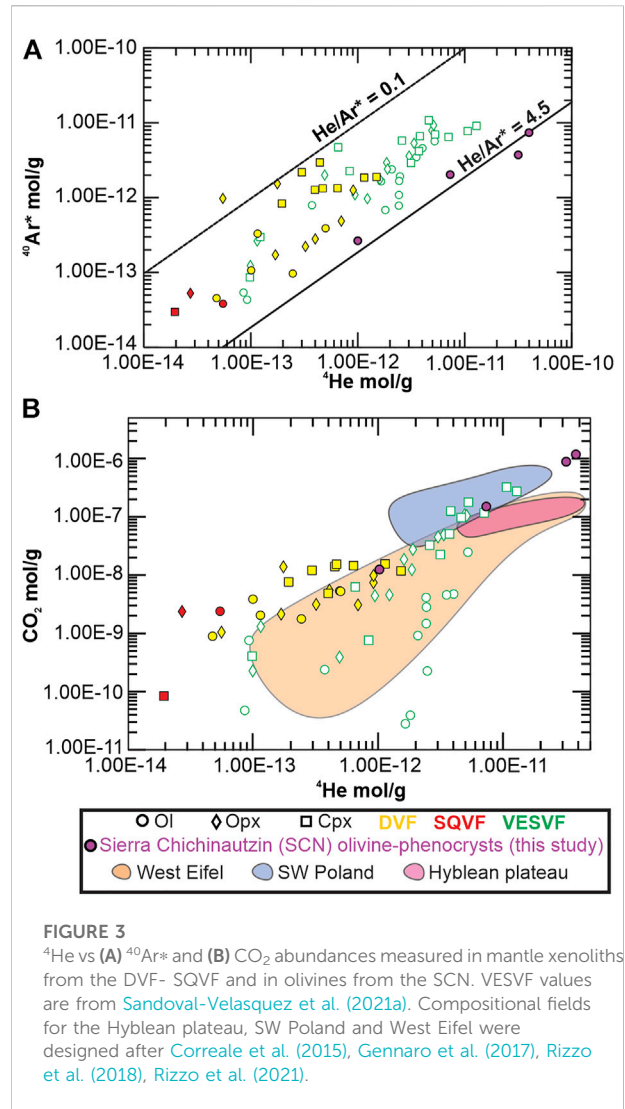


FIGURE 3
 ${}^4\text{He}$ vs (A) ${}^{40}\text{Ar}^*$ and (B) CO_2 abundances measured in mantle xenoliths from the DVF- SQVF and in olivines from the SCN. VESVF values are from Sandoval-Velasquez et al. (2021a). Compositional fields for the Hyblean plateau, SW Poland and West Eifel were designed after Correale et al. (2015), Gennaro et al. (2017), Rizzo et al. (2018), Rizzo et al. (2021).

ratios observed in the SQVF nodules. Pyroxenes generally show lower ${}^3\text{He}/{}^4\text{He}$ ratios than olivines, except for sample NMNH-37 Cpx that exhibits the highest ratio of the dataset (8.40 Ra; Table 2 and Figure 4A). Xenoliths from both localities do not exhibit systematic differences in air-normalized ${}^4\text{He}/{}^{20}\text{Ne}$ (X values) and ${}^4\text{He}/{}^{40}\text{Ar}^*$ ratios (Figure 4B), which range from 36.0 to 645.1 and from 0.1 to 2.5, respectively. ${}^{40}\text{Ar}/{}^{36}\text{Ar}$ ratios measured in all samples are higher than in atmosphere (298.56), but the maximum value (1,031) is much lower than in Mid-ocean Ridge Basalts (MORB, $\sim 44,000$; Moreira et al., 1998). ${}^{20}\text{Ne}/{}^{21}\text{Ne}$ and ${}^{21}\text{Ne}/{}^{22}\text{Ne}$ values vary from 9.80 ± 0.01 (1σ) to 12.57 ± 0.10 (1σ) and from 0.0290 ± 0.0003 (1σ) to 0.056 ± 0.0024 (1σ), respectively. The carbon isotopic composition of CO_2 ($\delta^{13}\text{C}$ values) reported for the DVF samples vary between -5.43% and -3.80% .

In SCN phenocrysts, FI are dominated by CO_2 and show the highest concentrations in the dataset (1.17×10^{-8} to 1.29×10^{-6} mol/g; Figure 3B). Helium concentrations are also high

compared to those in mantle xenoliths: ^3He and ^4He contents vary from 9.98×10^{-18} to 3.94×10^{-16} and from 1.00×10^{-12} to 3.99×10^{-11} mol/g, respectively. Rc/Ra ($7.15 \pm 0.14 \text{ Ra}$) and $^4\text{He}/^{40}\text{Ar}^*$ ratios (ranging between 3.68 and 8.71) are within the MORB range with $^4\text{He}/^{40}\text{Ar}^*$ ratios being higher than those observed in Mexican xenoliths. In general, samples exhibit $^4\text{He}/^{20}\text{Ne} > 10,000$ (X values) and $^{40}\text{Ar}/^{36}\text{Ar} > 650$ (except for sample MCH06-5) and $\delta^{13}\text{C}$ values between -6.31 and -5.00% .

6 Discussion

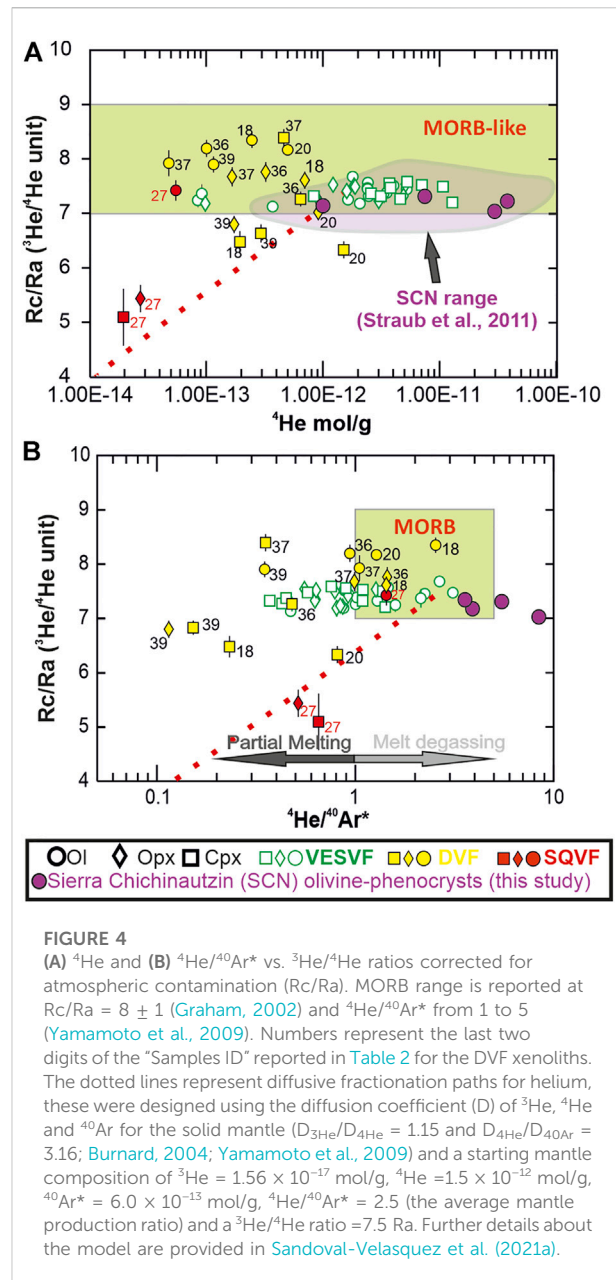
6.1 The upper mantle noble gas signature of the Mexican Basin and Range Province

6.1.1 The residual nature of the mantle source

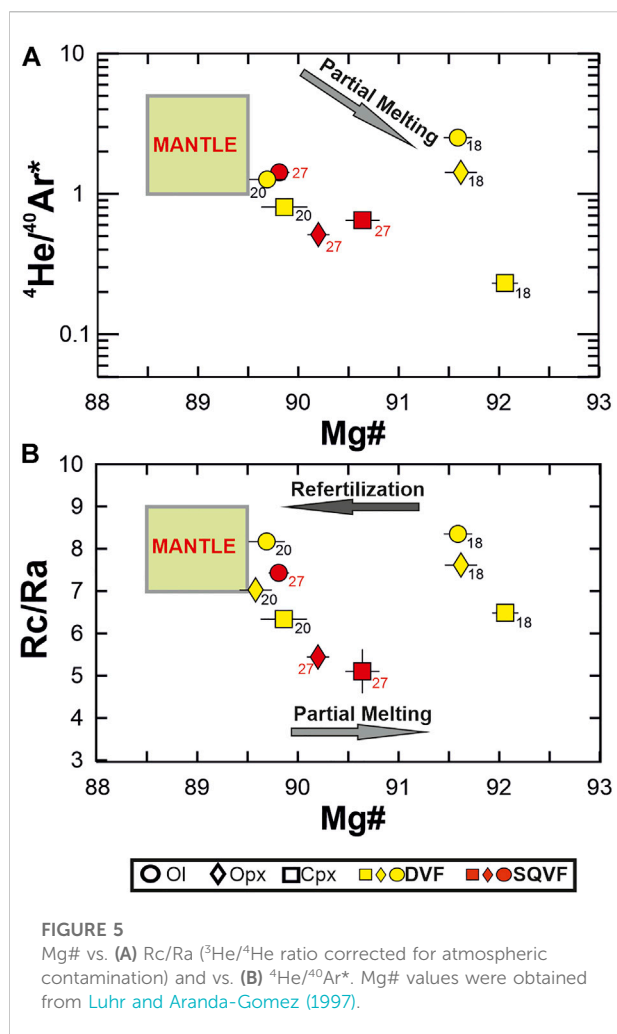
The petrology and geochemistry of the mantle xenoliths studied here have previously been interpreted (Luhr and Aranda-Gomez, 1997) as evidence of a complex evolution of the Mexican Basin and Range source mantle, in which episodes of partial melting and/or metasomatism have occurred. As shown in Figure 5, most inclusions-hosting crystals have Mg# values well above the typical fertile mantle range (88.5–89.5), indicating a residual nature of the mantle source, e.g., that the mantle has suffered extensive partial melting.

Partial mantle melting can impact the mantle noble gas signature (recorded in FI) in many different ways. Firstly, noble gases have different affinities for crystal and melt. Indeed, the olivine/melt distribution coefficients of Ar and He are $^{40}\text{Ar}/^{40}\text{Ar}^{\text{min/melt}} = 0.0011 \pm 0.0006$ and $^4\text{He}/^4\text{He}^{\text{min/melt}} = 0.00017 \pm 0.00013$, while for the cpx/melt system are $^{40}\text{Ar}/^{40}\text{Ar}^{\text{min/melt}} = 0.0011 \pm 0.0007$ and $^4\text{He}/^4\text{He}^{\text{min/melt}} = 0.0002 \pm 0.0002$ (Heber et al., 2007). The more incompatible (lower mineral/melt distribution coefficients) nature of He (relative to Ar) implies that He can more effectively escape from the mantle during partial melting, causing a decrease of the $^4\text{He}/^{40}\text{Ar}^*$ of the mantle residuum (Burnard, 2004; Heber et al., 2007; Yamamoto et al., 2009). The $^4\text{He}/^{40}\text{Ar}^*$ population of our samples supports the partial melting hypothesis (Figure 5A). While Ol crystals (having more refractory behavior during melting) exhibit $^4\text{He}/^{40}\text{Ar}^*$ ratios well within the mantle production range, four out of five pyroxenes exhibit decreasing $^4\text{He}/^{40}\text{Ar}^*$ ratios at increasing Mg# (Figure 5A).

Secondly, partial melting can also impact the helium isotopic signature by triggering diffusive fractionation processes (Burnard, 2004; Yamamoto et al., 2009). Noble gases can diffuse in minerals during the formation of melt-filled dissolution channels in the mantle as a result of partial melting or metasomatic episodes. This process, mainly affecting spinel and pyroxenes (Burnard, 2004; Yamamoto et al., 2009; Faccini et al., 2020), leads to isotopic fractionation because of the mass dependency of diffusion, which causes the lighter ^3He to diffuse faster than ^4He ($D_{^3\text{He}}/D_{^4\text{He}} = 1.15$; Trull



and Kurz, 1993; Burnard, 2004; Yamamoto et al., 2009). Similarly, ^4He will escape faster than $^{40}\text{Ar}^*$ ($D_{^4\text{He}}/D_{^{40}\text{Ar}} = 3.16$; Burnard, 2004; Yamamoto et al., 2009). Diffusive fractionation therefore ultimately results in He-depleted, lower $^3\text{He}/^4\text{He} - ^4\text{He}/^{40}\text{Ar}^*$ compositions in the mantle/magma residuum. Again, four out of six pyroxenes in our sample suite exhibit lower $^3\text{He}/^4\text{He}$ ratios than the MORB-like upper mantle range (Figure 5B); samples from the SQVF (red symbols) exhibit an especially evident decrease in $^3\text{He}/^4\text{He}$ accompanied by a depletion in ^4He concentrations and $^4\text{He}/^{40}\text{Ar}^*$ (Figures 4A,B) that point to diffusive fractionation. We modeled this process using the methodology of Sandoval-



Velasquez et al. (2021a), and find that the fractionation trend (see dashed red lines in Figure 4) reproduces well the He-poor, low $^3\text{He}/^4\text{He}$ signature SQVF pyroxenes, and of Cpx from nodules NMNH-20, and NMNH-18. It is also very possible that diffusive fractionation may have (at least partly) impacted the composition of samples NMNH-36 Cpx and NMNH-39 Opx/Cpx (Figure 4) as observed in some VESVF samples (Sandoval-Velasquez et al., 2021a).

Ultimately, we argue that melting-triggered diffusive fractionation is likely to have altered the pristine (pre-melting) He isotopic signature of samples NMNH-20 Opx/Cpx, NMNH-18 Cpx, NMNH-27 Opx/Cpx, and to a minor extent NMNH-36 Cpx and NMNH-39 Opx/Cpx. These samples are not considered further in the following sections.

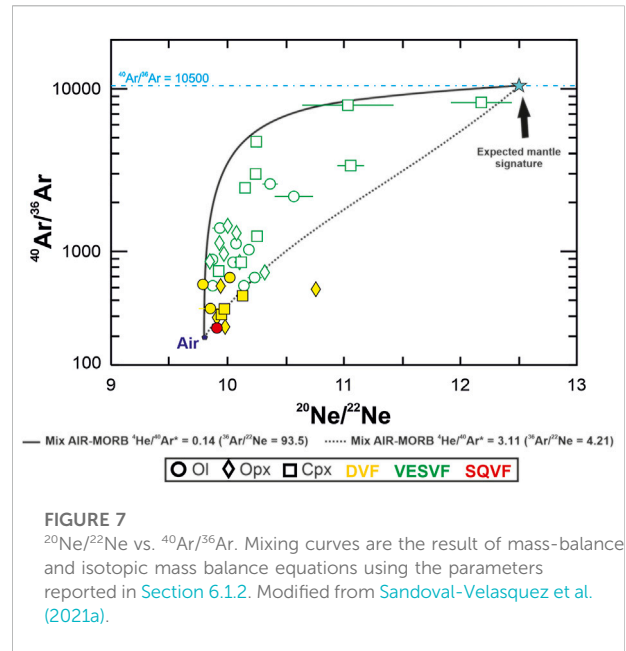
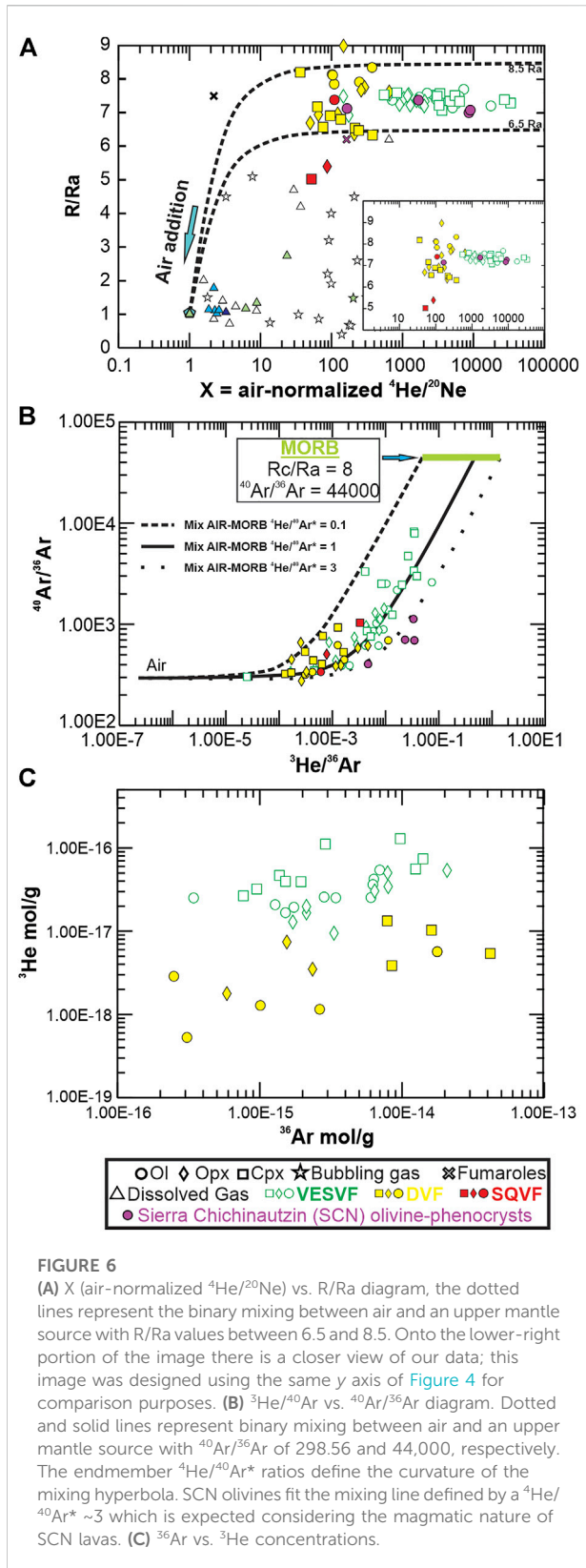
6.1.2 A slab-recycled atmospheric component in the mantle

Neon and argon isotopes measured in mantle rocks generally reflect mixing between mantle and atmospheric fluids that

suggests a contamination of FI by air-derived noble gases (Farley and Poreda, 1993; Matsumoto et al., 2001; Graham, 2002; Ozima and Podosek, 2002; Hopp et al., 2007a; Martelli et al., 2011; Rizzo et al., 2018; Rizzo et al., 2021). While atmospheric contamination of FI can occur during eruption of the transporting magmas, or during exposure of mantle xenoliths to the surface, the recycling of atmospheric gases into the local mantle has also been proposed. Holland and Ballentine (2006) demonstrate that significant quantities of seawater-derived noble gases are continuously introduced into the convective mantle during subduction. Besides, Hopp et al. (2007a), Matsumoto et al. (2002), Rizzo et al. (2018), Rizzo et al. (2021), and Sandoval-Velasquez et al. (2021b) suggest the existence of recycled atmospheric fluids in the Subcontinental Lithospheric mantle (SCLM; even far from present-day subduction zones) based on analysis of $^3\text{He}/^{36}\text{Ar}$, $^4\text{He}/^{20}\text{Ne}$, $^{20}\text{Ne}/^{22}\text{Ne}$, $^{21}\text{Ne}/^{22}\text{Ne}$, $^{36}\text{Ar}/^{22}\text{Ne}$ and $^{40}\text{Ar}/^{36}\text{Ar}$ ratios in FI trapped in ultramafic xenoliths. These studies prove the long-term preservation of air-derived noble gases in the SCLM located beneath intraplate settings, and invoke the effect of paleo-subduction events to explain the presence of these recycled atmospheric components in the mantle.

Our air-normalized $^4\text{He}/^{20}\text{Ne}$ (X values) vs. R/Ra ($^3\text{He}/^4\text{He}$ ratio not corrected for atmospheric contamination) and $^3\text{He}/^{36}\text{Ar}$ vs. $^{40}\text{Ar}/^{36}\text{Ar}$ diagrams (Figures 6A,B) clearly support mixing between mantle and atmospheric fluids. When compared with the VESVF xenoliths, DVF and SQVF nodules show lower $^4\text{He}/^{20}\text{Ne}$ and $^{40}\text{Ar}/^{36}\text{Ar}$ ratios; on average, DVF xenoliths exhibit $^4\text{He}/^{20}\text{Ne}$ of 172.9 ± 149.4 and $^{40}\text{Ar}/^{36}\text{Ar}$ of 462.5 ± 128.5 (1σ); while the VESVF xenoliths show $^4\text{He}/^{20}\text{Ne}$ of $4,324.9 \pm 6,812.9$ and $^{40}\text{Ar}/^{36}\text{Ar}$ of 1962.5 ± 1958.5 (1σ). Besides, as in the case of the VESVF xenoliths (Sandoval-Velasquez et al., 2021a), ^3He and ^{36}Ar abundances are correlated (Figure 6C), supporting the hypothesis that the atmospheric component identified in DVF and SQVF nodules has been trapped at mantle conditions (e.g., Matsumoto et al., 2001).

Sandoval-Velasquez et al. (2021a) previously inferred the isotopic characteristics of the Mexican SCLM by applying the approach developed by Langmuir et al. (1978) and Hopp et al. (2007a) to the VESVF mantle nodules. Using this methodology, they estimated a $^{40}\text{Ar}/^{36}\text{Ar}$ of $\sim 10,500$ for the Mexican SCLM (with $^4\text{He}/^{20}\text{Ne}$ ratios $< 40,000$) (Figure 6A). We find (Figure 7) that the SQVF and DVF FI fit the same model previously presented for the VESVF, therefore suggesting that the deep recycled atmospheric component is a regional (and not local) feature. We propose this regional atmospheric component to arise from subduction-related contamination of the Mexican SCLM during the eastward descent of the Farallon slab beneath the North American plate (~ 70 – 11 Ma ago), driven by the release of slab derived oxidized hydrous fluids or water-bearing silicate melts as proposed for present-day subduction zones (Wood et al., 1990; Luhr and Aranda-Gomez, 1997; Parkinson and Arculus, 1999; Kelley and Cottrell, 2009).



6.1.3 $^3\text{He}/^4\text{He}$ signature of the mantle beneath DVF and SQVF

The average $^3\text{He}/^4\text{He}$ ratio of the lithospheric mantle beneath the DVF is $8.39 \pm 0.24 \text{ Ra}$ (1σ). In the case of the SQVF, only the olivine aliquot is representative of the local mantle, and has a $^3\text{He}/^4\text{He}$ ratio = $7.39 \pm 0.20 \text{ Ra}$ (Figure 4A). Both values fall within the MORB-like upper mantle range, which excludes the influence of a lower mantle component (plume hypothesis) beneath these localities (Rc/Ra values above nine are commonly associated to mantle plume localities such as Hawaii, Iceland, the East African Rift or the Canary Islands; Vance et al., 1989; McMurtry et al., 2019; Day and Hilton, 2020; Halldórsson et al., 2022). These results corroborate the hypothesis that the Quaternary monogenetic volcanism of the DVF and the SQVF was produced by continental extension.

The estimated $^3\text{He}/^4\text{He}$ average composition ($8.39 \pm 0.24 \text{ Ra}$) for DVF samples is less radiogenic than seen at other Basin and Range mantle xenolith-bearing localities, including VESVF (Figure 4A). Sandoval-Velasquez et al. (2021a) invoked a role of the subducted Farallon plate to explain the $^3\text{He}/^4\text{He}$ signature of VESVF xenoliths. In their hypothesis, the retreating of the Farallon slab ($\sim 40 \text{ Ma}$ ago) triggered the refertilization of the lithospheric mantle through the injection of ^3He -rich asthenospheric melts (Lee, 2005; Nieto-Samaniego et al., 2005). Because of the relative proximity between the DVF and the VESVF, a similar geodynamic processes is expected (Figure 8). If we consider the tectonic configuration of the western margin of North America at the time of the Laramide

Orogeny (74–40 Ma), in which the Farallon plate acted as a natural barrier between the lithospheric mantle and the asthenosphere (Figure 8B), it is reasonable to suppose that during the subsequent rollback and retreating, the VESVF mantle was exposed to, and refertilized by, the hot asthenosphere first (40–20 Ma ago Figure 8C); since then, the VESVF lithospheric mantle would have evolved in steady-state (Gautheron and Moreira, 2002), gradually becoming more radiogenic (due to ^4He production by decay of U-Th isotopes) during the last 20 Ma (starting from a $^3\text{He}/^4\text{He}$ ratio ~ 8.5 Ra, which is close to the highest ratio reported in our Mexican mantle xenoliths). As the retreating process continued, the mantle beneath the DVF would have been refertilized at a later stage, which might explain the higher $^3\text{He}/^4\text{He}$ ratios observed there. These arguments imply a shorter residence time ($Rt < 20$ Ma) of helium (less production of radiogenic ^4He) for the DVF subcontinental mantle when compared with the VESVF results (Sandoval-Velasquez et al., 2021a; Figures 8D,E).

The above hypothesis can be tested estimating the refertilization age of the DVF mantle following the formula proposed by Ballentine and Burnard (2002) for the ^4He production rate:

$$^4\text{He atoms } g^{-1} \text{ yr}^{-1} = (3.115 \times 10^6 + 1.272 \times 10^5) [U] + 7.710 \times 10^5 [\text{Th}] \quad (5)$$

where [U] and [Th] are Uranium and Thorium concentrations in ppm. Assuming a U concentration between 0.01 and 0.03 ppm (and a Th/U = 3; Gautheron and Moreira, 2002) for the Mexican mantle xenoliths (Dávalos-Elizondo et al., 2016), it is possible to estimate a ^4He production rate between 9.23×10^{-20} and 2.77×10^{-19} mol/g \cdot yr. Considering a steady-state model (same as proposed for the VESVF; Sandoval-Velasquez et al., 2021a) for the lithospheric mantle beneath the DVF, the above-estimated ^4He production rate, a starting $^3\text{He}/^4\text{He} = 8.5$ Ra, and ^4He concentration = 4.5×10^{-11} mol/g (the maximum value identified for continental mantle xenoliths; Gautheron and Moreira, 2002), we estimate that a residence time (Rt) of 4 to 10 Ma is needed to decrease the helium ratio from 8.5 to 8.39 Ra (the average $^3\text{He}/^4\text{He}$ values measured in DVF xenoliths). In other words, these ages support the idea that the DVF mantle was more recently refertilized than the mantle located beneath the VESVF, where a Rt of 40–20 Ma was estimated previously (Sandoval-Velasquez et al., 2021a). This would explain the higher $^3\text{He}/^4\text{He}$ ratios observed in Ol and Opx crystals from DVF xenoliths.

The SQVF $^3\text{He}/^4\text{He}$ ratio signature falls within the VESVF mantle range. Considering the steady-state model previously discussed, the most plausible explanation for the similarity in helium isotope compositions between SQVF and VESVF is that

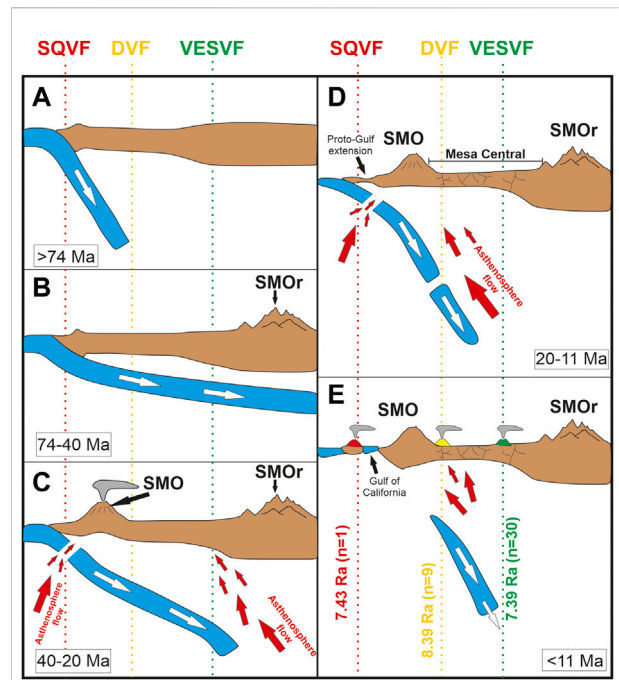


FIGURE 8

Evolution of the western margin of the North American plate during the Late Mesozoic and Cenozoic. (A) Subduction of the Farallon slab beneath North America during the Mesozoic. (B) Shallowing of the subduction angle and tectonic uplift of the Sierra Madre Oriental (SMOr; Laramide Orogeny). (C) Rollback and first break-off of the Farallon slab causing the introduction of asthenospheric fluids in the lithospheric mantle beneath the SQVF and VESVF. This process caused extensional deformation in the Basin and Range Province, refertilization of the lithospheric mantle and the second ignimbrite flare-up of the Sierra Madre Occidental (SMO). (D) Over time, the subduction angle increased and ceased triggering a second break-off episode and the subsequent Proto-Gulf extension. Second refertilization event beneath SQVF? (E) The lithospheric mantle beneath the DVF is finally refertilized. Subduction ends in the western margin of Mexico and the SCLM beneath SQVF, DVF, and VESVF evolves in steady-state becoming more radiogenic over time. The Basin and Range extension facilitated the formation of mantle xenolith-bearing alkali basalt localities (e.g., the VESVF, SQVF, and DVF) in the Mesa Central and the Baja California Peninsula. Adapted from Lee (2005).

the mantle beneath both localities was refertilized at similar ages. In the case of a normal slab rollback, mantle refertilization should have in principle proceeded from east to west; therefore, in this scenario, the SQVF mantle should have been the last mantle portion to be refertilized by the asthenospheric melts. If this was the case, however, the $^3\text{He}/^4\text{He}$ signature of the SQVF mantle should be at least equal to (or even higher than) the DVF average (8.5Ra), which is opposite to what we observe.

To explain this low $^3\text{He}/^4\text{He}$ signature of SQVF, we turn our attention into the possible role played by the Farallon slab break-off (Figure 8C). According to Ferrari et al. (2012), the old Mexican magmatic arc i.e., the Sierra Madre Occidental (SMO; Figure 8B; Ferrari et al., 1999; Ferrari et al., 2002; Nieto-Samaniego et al., 1999), was generated in two different

episodes of ignimbrite flare-up: the first occurred in the Oligocene (31.5–28 Ma) and the second during the Miocene (23.5–20 Ma). Ferrari et al. (2002) link the second episode of volcanism to a detachment (or break-off) of the Farallon slab that also promoted an extensional deformation in southern Baja California and central Mexico before the opening of the Gulf of California. During this break-off (Figure 8C; 24–20 Ma; Ferrari et al., 2002) the cold lithosphere would have been replaced by the hotter asthenosphere which abruptly increased the temperature at the base of the crust triggering the refertilization of the lithospheric mantle and the generation of silicic crustal magmas via mafic underplating. Subsequently, a second slab break-off would have occurred in the middle Miocene (~14–11 Ma; Figure 8D) inducing a new extensional phase that probably triggered a new intrusion of the asthenosphere in the SCLM, the proto-Gulf extension, the partial melting of the mantle right below the present-day Gulf of California and the eruption of mafic melts that characterized the late Miocene mafic volcanism in the eastern side of the Gulf (Henry and Aranda-Gomez, 2000; Ferrari et al., 2002).

Ultimately, these break-off events may explain well why the SQVF mantle was refertilized synchronously with the VESVF and much earlier than DVF mantle (Figures 8C,D), ultimately justifying its relatively radiogenic He signature.

6.2 Noble gas signature of SCN volcanism

The lavas from SCN studied in this work have relatively high Mg# (>60) and $^3\text{He}/^4\text{He}$ ratios within the MORB-like upper mantle range (Figure 4), so it is reasonable to assume that the FI hosted in our olivine separates are (at least to some extent) representative of the fluids present in the SCN sub-arc mantle, as petrological observations suggest (Mg# ~70, MgO between 7.15 and 9.60 wt% and high Ni >100 ppm; Straub et al., 2011). A comparison with data obtained for the VESVF, DVF, and SQVF xenoliths is therefore justified.

Olivines from the calc-alkaline basaltic andesites (samples CH09-1 and CH09-9) exhibit the highest He and CO_2 concentrations in our Mexican dataset ($^4\text{He} = 2.46 \times 10^{-11}$ — $\text{CO}_2 = 7.17 \times 10^{-7}$ mol/g and $^4\text{He} = 3.99 \times 10^{-11}$ — $\text{CO}_2 = 1.29 \times 10^{-6}$ mol/g, respectively; Table 2 and Figure 3); samples CH05-16 and MCH06-5 (high-Nb basalts) exhibit higher concentrations ($^4\text{He} = 7.26 \times 10^{-12}$ — $\text{CO}_2 = 1.60 \times 10^{-7}$ mol/g and $^4\text{He} = 1.00 \times 10^{-12}$ mol/g— $\text{CO}_2 = 1.17 \times 10^{-8}$ mol/g, respectively) than in DVF and the SQVF nodules and comparable contents relative to the VESVF mantle xenoliths. The fact that SCN olivines exhibit gas concentrations comparable to, or even higher than, the VESVF nodules indicate a volatile-rich parental melt or entrapment depth of FI higher than in the mantle xenoliths. We believe that the hypothesis of a deeper entrapment of FI is unrealistic since relatively low Mg# that ranges from 60 to 70 and high $^4\text{He}/^{40}\text{Ar}^*$ ratios >3 confirm the magmatic nature of our olivines. Despite the differences in gas contents observed in CH09-1 and CH09-9, all SCN

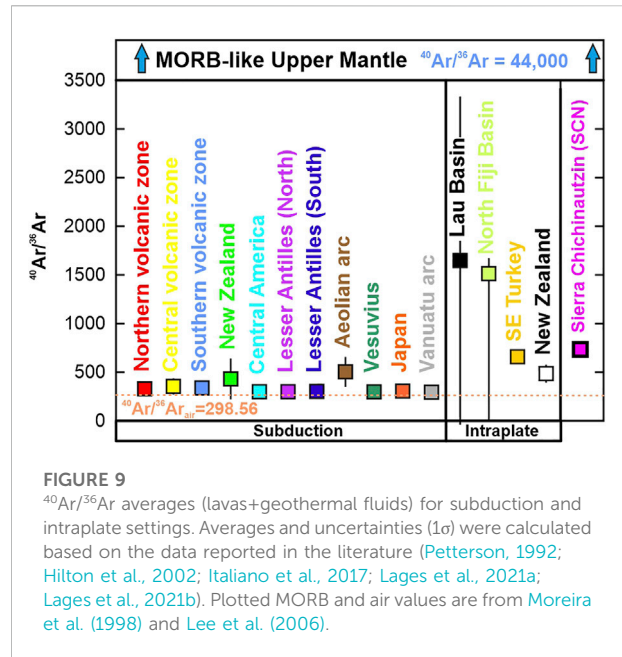


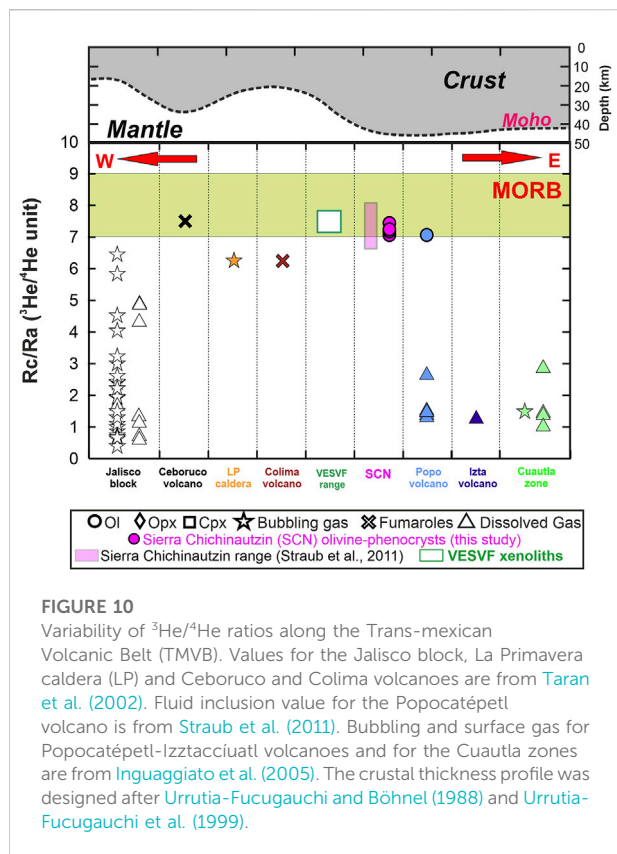
FIGURE 9

$^{40}\text{Ar}/^{36}\text{Ar}$ averages (lavas+geothermal fluids) for subduction and intraplate settings. Averages and uncertainties (1 σ) were calculated based on the data reported in the literature (Pettersson, 1992; Hilton et al., 2002; Italiano et al., 2017; Lages et al., 2021a; Lages et al., 2021b). Plotted MORB and air values are from Moreira et al. (1998) and Lee et al. (2006).

samples exhibit regular R_c/R_a values comparable to the xenoliths from VESVF (on average 7.24 ± 0.33 R_a; 1 σ) (Figure 4), suggesting that the olivines derive from an upper mantle with a similar signature.

Both basaltic andesites and alkaline basalts show higher $^4\text{He}/^{40}\text{Ar}^*$ ratios than those observed in mantle xenoliths (Figure 4B), consistent with the magmatic nature of fluids entrapped in the olivine-phenocryst; during degassing of silicate melts, preferential early removal of Ar (which is less soluble than He during melt degassing processes) can lead to later trapping of fluids with high $^4\text{He}/^{40}\text{Ar}^*$ ratios (Jambon et al., 1985; Burnard et al., 1997; Moreira and Sarda, 2000; Paonita and Martelli, 2007; Boudoire et al., 2018). It is worth noting that SCN olivine samples exhibit $^4\text{He}/^{20}\text{Ne}$ and $^{40}\text{Ar}/^{36}\text{Ar}$ falling within the range for VESVF mantle xenoliths, and along the mantle-air mixing trends (Figures 6A,B). Given the magmatic nature of the olivines, we cannot discard that the atmospheric component observed in SCN inclusions has been trapped at crustal depths; unlike helium, heavier noble gases (such as Ne and Ar) have accumulated in the atmosphere over the Earth's history, to the point that atmospheric contamination challenges interpretation of isotopic ratios, particularly in magmatic products (Farley and Poreda, 1993; Farley and Neroda, 1998; Graham, 2002; Mukhopadhyay and Parai, 2019). Despite the above, the similarity with VESVF noble gas ratios is clear and suggests that SCN olivines are (to some extent) reflecting the signature (Ne-Ar ratios) of the local mantle.

According to petrological evidence (Straub et al., 2011), the SCN lavas derive from a sub-arc mantle affected by the infiltration of silicic crustal material from the subducted slab to the point that secondary pyroxenite veins formed. If SCN magmas were completely related to subduction, then the fluid



inclusion data should exhibit $^{40}\text{Ar}/^{36}\text{Ar}$ ratios similar to those observed in lavas and geothermal fluids from other “classic” subduction systems which generally exhibit $^{40}\text{Ar}/^{36}\text{Ar} < 400$ (e.g., Andes, Lesser Antilles or Japan; Hilton et al., 2002; Lages et al., 2021a; Lages et al., 2021b). Figure 9 is a comparison of a selection of published $^{40}\text{Ar}/^{36}\text{Ar}$ averages for volcanic products from both subduction and intraplate settings worldwide. As observed, the average for SCN samples is higher than observed in subduction areas but is comparable to those ratios reported in zones where volcanism is related to intraplate extensional tectonics. Based on this evidence, we propose that SCN olivines reflect both subduction (as suggested by petrological data) and intraplate-related components (the latter with $^{40}\text{Ar}/^{36}\text{Ar}$ comparable to those reported for the VESVF mantle).

We conclude that, in terms of the gas concentrations and noble gas isotopic ratios, the SCN olivines reflect a sub-arc mantle with similar characteristics to those described for the VESVF mantle (Table 2; Figures 3, 4A, 6A, 10). It is therefore possible that both localities evolved under similar geodynamic conditions due to their proximity (Figure 1).

6.2.1 Comparison with noble gas information for the TMVB

Our observations, with those of Straub et al. (2011), are among the first fluid inclusion results available for the TMVB, while the majority of the isotopic data previously reported in the

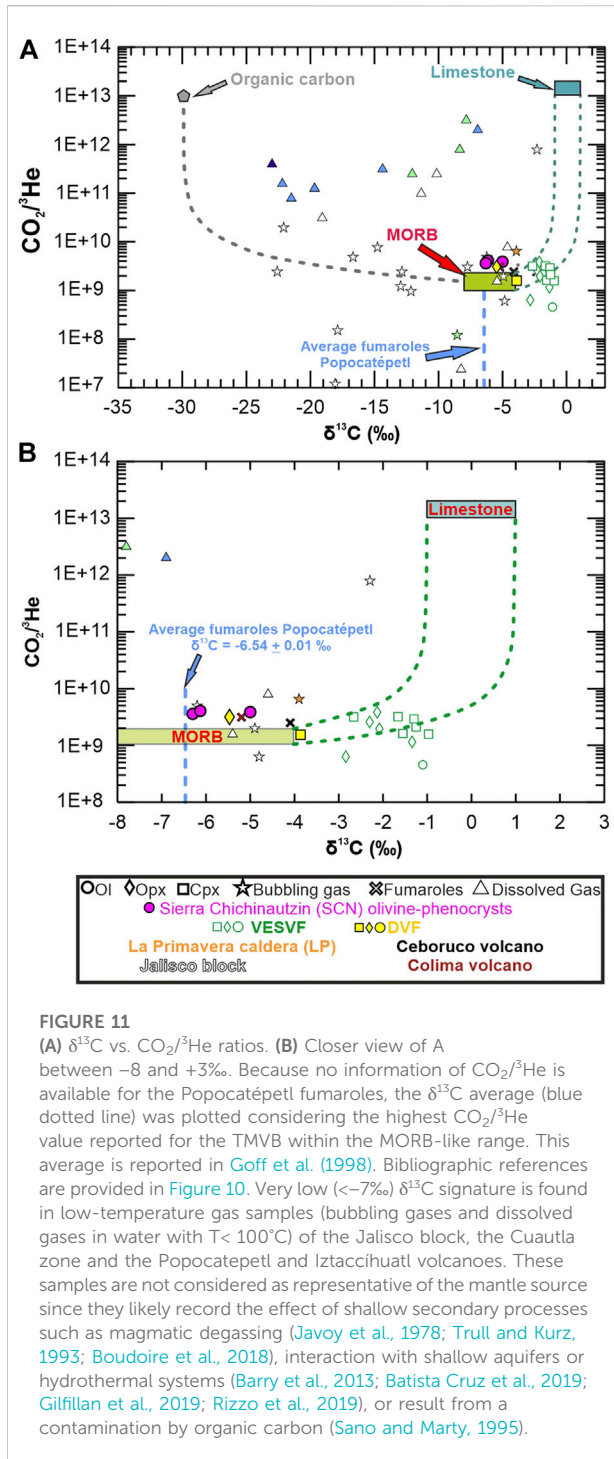
literature are from analysis of superficial gas emissions such as fumaroles, bubbling and dissolved gases (e.g., Taran et al., 2002; Inguaggiato et al., 2005). However, the representativeness of these surficial gas emissions for understanding the feeding mantle source characteristics is increasingly questioned (Lages et al., 2021a; Lages et al., 2021b). Therefore, a comparison between FI (this work and Straub et al., 2011) and TMVB surficial gases is timely and useful.

The available information for the TMVB is presented in Figures 6A, 10, and includes samples collected in the Jalisco block, Colima and Ceboruco volcanoes, La Primavera caldera, Popocatepetl and Iztacciatl volcanoes, and the Cuautla zone (for their location see Figure 1B). In the $^4\text{He}/^{20}\text{Ne}$ vs. R/Ra plot (Figure 6A), it is straightforward to distinguish FI from superficial gases, with the latter typically exhibiting lower $^3\text{He}/^4\text{He}$ and X values. Our results therefore confirm that volatiles sampled in peripheral geothermal fields and/or low-temperature bubbling springs are affected by shallow contamination from meteoric, biogenic fluids that result in lower $^3\text{He}/^4\text{He}$ signatures than in FI (and high-temperature fumarole emissions; Sano et al., 1984; Williams et al., 1987; Lages et al., 2021a). These processes are especially relevant for dissolved water samples that also exhibit the lowest $^4\text{He}/^{20}\text{Ne}$ ratios (very close to the $^4\text{He}/^{20}\text{Ne}$ air value = 0.318; Ozima and Podosek, 2002) confirming a dominant contamination of surficial gases by atmospheric-derived gases. In the case of Popocatepetl volcano, the difference in R/Ra between FI and dissolved water (Figure 10) demonstrates the utility of the former to investigate the source mantle helium isotopic signature. Bubbling/dissolved gas samples from the Jalisco block and the Cuautla zone show extremely low $^3\text{He}/^4\text{He}$ ratios, with averages of 2.24 ± 1.69 Ra (1σ) and 1.66 ± 0.70 Ra (1σ), respectively. Thus, we consider that bubbling and dissolved gas data observed in Figures 6A, 10 underestimate the real $^3\text{He}/^4\text{He}$ signature of the local mantle.

6.3 Insights into the $\delta^{13}\text{C}$ signature of the Mexican lithospheric mantle

Our $\delta^{13}\text{C}$ results for the DVF samples (NMNH-39 Opx and Cpx) fall within the MORB-like range (between -5.43% and -3.80% ; Figures 11A,B), and bring therefore no evidence of the isotopically heavy, recycled crustal carbon component identified in the VESVF samples (Sandoval-Velasquez et al., 2021a). We propose that the fertile $\delta^{13}\text{C}$ signature of the DVF mantle likely reflects the addition of MORB-type carbon during the recent (<11 Ma) mantle refertilization event by asthenospheric fluids (Figure 8E). This event may have masked any recycled crustal carbon signature eventually present in the local SCLM. In any case, the DVF vs. VESVF dichotomy points to $\delta^{13}\text{C}$ mantle heterogeneities at regional scale.

SCN olivines likewise show a MORB-like upper mantle $\delta^{13}\text{C}$ signature (Figure 11). Popocatepetl crater fumaroles (T. Lorenson and W. C. Evans, unpublished, as cited in Goff



et al., 1998), bubbling gas data from La Primavera Caldera, and high-temperature (840°C) fumaroles of Colima volcano (Taran et al., 2002) exhibit similar MORB-type carbon (Figure 11). This negative ^{13}C signature observed in SCN samples (relative to VESVF) can be explained by two distinct processes, taking in mind that crustal contamination in SCN lavas is thought to be

negligible (see Section 3). On the one hand, it is possible that SCN olivines (and Colima/Popocatepetl gases) record an isotopically fractionated CO_2 derived by magmatic degassing. Carbon isotopes are fractionated by magmatic degassing (melt-vapor fractionation factor Δ : from $+1.8$ to $+4.5$; Javoy et al., 1978; Matthey, 1991; Aubaud et al., 2005; Paonita et al., 2012; Gennaro et al., 2017; Boudoire et al., 2018), so that residual melts that result from late-stage degassing are ^{12}C -enriched (relative to parental, mantle-derived melts) because of preferential ^{13}C loss to magmatic vapor (Javoy et al., 1978; Boudoire et al., 2018). The high ${}^4\text{He}/{}^{40}\text{Ar}^*$ values ($3-9$) measured in FI of SCN olivines, well above the range observed in mantle xenoliths ($3.1 > {}^4\text{He}/{}^{40}\text{Ar}^* > 0.1$), are consistent with the magmatic degassing hypothesis. In this interpretation, the SCN inclusions (and possibly those from Popocatepetl and Colima volcanoes) would derive from extensive degassing of silicate parental melt with an originally heavier $\delta^{13}\text{C}$ signature, similar to that observed in VESVF xenoliths. Alternatively, if we accept that the negative $\delta^{13}\text{C}$ of SCN inclusions is source-related (i.e., that magmatic degassing plays a minor role), then the inferred sub-arc source at -4‰ to -7‰ would imply a negligible contribution of subduction-derived crustal carbon. This hypothesis would be consistent with the carbon data reported for other arc volcanoes such as Ceboruco, La Primavera and the neighbor Popocatepetl (Goff et al., 1998; Taran et al., 2002). In fact, Goff et al. (1998), Goff et al. (2001) and Aiuppa et al. (2017), indicate that the CO_2 -rich plume gases, emitted by Popocatepetl, are not directly related to subducted sediments (that are not C-rich at the Mexican trench; Plank, 2014), instead, it is the result of assimilation of crustal carbon materials (metamorphosed carbonate rocks).

7 Conclusion

The study of noble gases and CO_2 in FI of mantle xenoliths from DVF and SQVF, together with a previous study on the VESVF, allowed investigating the noble gas and carbon isotopic signatures in the Mexican lithospheric mantle. In addition, olivine phenocrysts from SCN gave the opportunity to extend the study to the present subduction-related volcanism of the TMVB. The main outcomes are:

- The decrease of ${}^4\text{He}/{}^{40}\text{Ar}^*$ ratios from olivines to pyroxenes in mantle xenoliths, coupled with a general increase in the Mg#, suggests a complex mantle source impacted by partial melting and/or metasomatic episodes;
- Ne and Ar systematics reveal mixing trends between atmospheric and MORB-like fluids. Based on the isotopic variability of our samples, mass-balance and isotopic mass balance equations were used in order to estimate the ${}^{40}\text{Ar}/{}^{36}\text{Ar}$ signature of the Mexican lithospheric mantle. DVF and SQVF samples confirm a

maximum $^{40}\text{Ar}/^{36}\text{Ar}$ of $\sim 10,500$ which supports the presence of an atmospheric component likely recycled via Farallon paleo-subduction.

- The inferred $^3\text{He}/^4\text{He}$ signature is 8.39 ± 0.24 Ra for the DVF xenoliths and 7.43 ± 0.19 Ra for SQVF xenoliths. Regional $^3\text{He}/^4\text{He}$ differences in the Basin and Range mantle are interpreted as the result of different ages of mantle refertilization caused by retreating of the Farallon slab (~ 40 Ma ago) and subsequent slab delamination (break-off) episodes. Using a steady-state model in which the mantle becomes more radiogenic over time, we propose that the VESVF and the SQVF source mantle was refertilized earlier (at 40-20 Ma) than the DVF mantle (<10 Ma).
- Fluids trapped in SCN olivines have $^3\text{He}/^4\text{He}$ signatures similar to VESVF mantle xenoliths and suggest that the mantle beneath the two areas evolved under similar geodynamic conditions. The $^3\text{He}/^4\text{He}$ ratios are relatively homogeneous in the mantle source underneath Mexico.
- Contrary to what was observed in the VESVF xenoliths, the carbon isotopic composition of CO_2 ($\delta^{13}\text{C}$ values) reported for the DVF samples are more negative (between -5.43% and -3.80%). As with helium ratios, these MORB-like carbon signatures are linked to the relatively recent refertilization event proposed for the DVF local mantle.
- $\delta^{13}\text{C}$ values measured in SCN samples also falls within the MORB-like range and are comparable to those reported for the Popocatepél, Ceboruco and Colima fumaroles and bubbling gas obtained from La Primavera caldera. Unlike the evidence found in VESVF, the $\delta^{13}\text{C}$ values in SCN and in the volcanoes from TMVB indicate that magmas likely result from the melting of mantle with a distinct carbon signature and content than that represented by VESVF xenoliths. This source would also show a negligible contamination by subduction-related crustal carbon.

Data availability statement

The original contributions presented in the study are included in the article, further inquiries can be directed to the corresponding author.

Author contributions

AS-V performed analyses of fluid inclusions, elaborated and interpreted data, conceptualized models, and wrote the final version of the manuscript. AR and AA contributed to

the conceptualization, methodology, writing-reviewing, editing, and supervision. SMS performed fieldwork, sampling, and write-reviewing. AG-T and RE-P helped with fieldwork and sampling. All authors contributed to manuscript revision, read, and approved the submitted version.

Funding

This research was funded by the Italian Minister (PRIN2017LMNLAW) and by the Deep Carbon Observatory.

Acknowledgments

This paper is part of the PhD (XXXIV cycle) of AS-V at the University of Palermo. We are extremely grateful to the Department of Mineral Sciences of the Smithsonian Institution for providing samples of Mexican mantle xenoliths from the Durango and San Quintin volcanic fields. We thank Mariano Tantillo and Mariagrazia Misseri for helping in sample preparation, the isotope analysis of noble gases and the CO_2 extraction from FI performed in the noble gas laboratory of INGV-Palermo. We are also grateful to Ygor Oliveri and Giorgio Capasso for their help in the CO_2 isotopic analysis performed in the INGV-Palermo stable isotopes laboratory. We wish to extend our special thanks to Prof. Paola Marianelli, Prof. Karoly Nemeth, and the Reviewer for their insightful comments and suggestions that improved our manuscript.

Conflict of interest

The authors declare that the research was conducted in the absence of any commercial or financial relationships that could be construed as a potential conflict of interest.

The reviewer MM declared a past co-authorship with the author RE-P to the handling editor.

Publisher's note

All claims expressed in this article are solely those of the authors and do not necessarily represent those of their affiliated organizations, or those of the publisher, the editors and the reviewers. Any product that may be evaluated in this article, or claim that may be made by its manufacturer, is not guaranteed or endorsed by the publisher.

References

- Aiuppa, A., Fischer, T. P., Plank, T., Robidoux, P., and Di Napoli, R. (2017). Along-arc, inter-arc and arc-to-arc variations in volcanic gas CO₂/ST ratios reveal dual source of carbon in arc volcanism. *Earth. Sci. Rev.* 168, 24–47. doi:10.1016/j.earscirev.2017.03.005
- Albritton, C. C. (1958). Quaternary stratigraphy of the guadiana valley, Durango, Mexico. *Geol. Soc. Am. Bull.* 69, 1197. doi:10.1130/0016-7606(1958)69[1197:QSOTGV]2.0.CO;2
- Aranda-Gómez, J. J., Henry, C. D., and Luhr, F. J. (2000). Evolución tectonomagmática post-paleocénica de la Sierra Madre Occidental y de la porción meridional de la provincia tectónica de Cuencas y Sierras, México. *Bol. Soc. Geol. Mex.* 53, 59–71. doi:10.18268/BSGM2000v53n1a3
- Aranda-Gómez, J. J., Luhr, J. F., and Pier, G. (1992). The La Breña — El Jagüey maar complex, Durango, México: I. Geological evolution. *Bull. Volcanol.* 54, 393–404. doi:10.1007/BF00312321
- Aranda-Gómez, J. J., and Ortega-Gutiérrez, F. (1987). “Mantle xenoliths in México,” in *Mantle xenoliths* (New York: John Wiley), 75–84.
- Atwater, T. (1989). “Plate tectonic history of the northeast Pacific and western North America,” in *The eastern pacific ocean and Hawaii*. Editors E. L. Winterer, D. M. Hussong, and R. W. Decker (North America: Geological Society of America), 21–72. doi:10.1130/DNAG-GNA-N.21
- Aubaud, C., Pineau, F., Hékinian, R., and Javoy, M. (2005). Degassing of CO₂ and H₂O in submarine lavas from the Society hotspot. *Earth Planet. Sci. Lett.* 235, 511–527. doi:10.1016/j.epsl.2005.04.047
- Ballentine, C. J., and Burnard, P. G. (2002). Production, release and transport of noble gases in the continental crust. *Rev. Mineral. Geochem.* 47, 481–538. doi:10.2138/rmg.2002.47.12
- Barry, P. H., Hilton, D. R., Fischer, T. P., de Moor, J. M., Mangasini, F., and Ramirez, C. (2013). Helium and carbon isotope systematics of cold “mazuku” CO₂ vents and hydrothermal gases and fluids from Rungwe Volcanic Province, southern Tanzania. *Chem. Geol.* 339, 141–156. doi:10.1016/j.chemgeo.2012.07.003
- Basu, A. R. (1977). Textures, microstructures and deformation of ultramafic xenoliths from San Quintin, Baja California. *Tectonophysics* 43, 213–246. doi:10.1016/0040-1951(77)90118-4
- Batista Cruz, R. Y., Rizzo, A. L., Grassa, F., Bernard Romero, R., González Fernández, A., Kretzschmar, T. G., et al. (2019). Mantle degassing through continental crust triggered by active faults: The case of the Baja California Peninsula, Mexico. *Geochem. Geophys. Geosyst.* 20, 1912–1936. doi:10.1029/2018GC007987
- Bekaert, D. V., Turner, S. J., Broadley, M. W., Barnes, J. D., Halldórsson, S. A., Labidi, J., et al. (2021). Subduction-driven volatile recycling: A global mass balance. *Annu. Rev. Earth Planet. Sci.* 49, 37–70. doi:10.1146/annurev-earth-071620-055024
- Boudoire, G., Rizzo, A. L., Di Muro, A., Grassa, F., and Liuzzo, M. (2018). Extensive CO₂ degassing in the upper mantle beneath oceanic basaltic volcanoes: First insights from Piton de la Fournaise volcano (La Réunion Island). *Geochim. Cosmochim. Acta* 235, 376–401. doi:10.1016/j.gca.2018.06.004
- Bunge, H.-P., and Grand, S. P. (2000). Mesozoic plate-motion history below the northeast Pacific Ocean from seismic images of the subducted Farallon slab. *Nature* 405, 337–340. doi:10.1038/35012586
- Burnard, P. (2004). Diffusive fractionation of noble gases and helium isotopes during mantle melting. *Earth Planet. Sci. Lett.* 220, 287–295. doi:10.1016/S0012-821X(04)00060-3
- Burnard, P., Graham, D., and Turner, G. (1997). Vesicle-specific noble gas analyses of “popping rock”: Implications for primordial noble gases in Earth. *Science* 276, 568–571. doi:10.1126/science.276.5312.568
- Correale, A., Martelli, M., Paonita, A., Rizzo, A., Brusca, L., and Scribano, V. (2012). New evidence of mantle heterogeneity beneath the Hyblean Plateau (southeast Sicily, Italy) as inferred from noble gases and geochemistry of ultramafic xenoliths. *Lithos* 132 (133), 70–81. doi:10.1016/j.lithos.2011.11.007
- Correale, A., Paonita, A., Rizzo, A., Grassa, F., and Martelli, M. (2015). The carbon-isotope signature of ultramafic xenoliths from the Hyblean Plateau (southeast Sicily, Italy): Evidence of mantle heterogeneity. *Geochem. Geophys. Geosyst.* 16, 600–611. doi:10.1002/2014GC005656
- Dasgupta, R., and Hirschmann, M. M. (2010). The deep carbon cycle and melting in Earth’s interior. *Earth Planet. Sci. Lett.* 298, 1–13. doi:10.1016/j.epsl.2010.06.039
- Dávalos-Elizondo, M. G., Aranda Gómez, J. J., Levresse, G., and Cervantes-de la Cruz, K. E. (2016). Química mineral y geoquímica de xenolitos del manto del campo volcánico Santo Domingo, san luis potosí: Evidencias de procesos metasomáticos del manto bajo porciones de la Mesa central, México. *Rev. Mex. Ciencias Geol.* 33, 81–104.
- Day, J. M. D., and Hilton, D. R. (2020). Heterogeneous mantle-derived helium isotopes in the Canary Islands and other ocean islands. *Geology* 49, 120–124. doi:10.1130/G47676.1
- Day, J. M. D., and Hilton, D. R. (2011). Origin of ³He/⁴He ratios in HIMU-type basalts constrained from Canary Island lavas. *Earth Planet. Sci. Lett.* 305, 226–234. doi:10.1016/j.epsl.2011.03.006
- Deines, P. (2002). The carbon isotope geochemistry of mantle xenoliths. *Earth. Sci. Rev.* 58, 247–278. doi:10.1016/S0012-8252(02)00064-8
- Dickinson, W. R. (2002). The Basin and range province as a composite extensional domain. *Int. Geol. Rev.* 44, 1–38. doi:10.2747/0020-6814.44.1.1
- Dunai, T. J., and Porcelli, D. (2002). Storage and transport of noble gases in the subcontinental lithosphere. *Rev. Mineral. Geochem.* 47, 371–409. doi:10.2138/rmg.2002.47.10
- Faccini, B., Rizzo, A. L., Bonadiman, C., Ntaflos, T., Seghedi, I., Grégoire, M., et al. (2020). Subduction-related melt refertilisation and alkaline metasomatism in the Eastern Transylvanian Basin lithospheric mantle: Evidence from mineral chemistry and noble gases in fluid inclusions. *Lithos* 364–365, 105516. doi:10.1016/j.lithos.2020.105516
- Farley, K. A., and Neroda, E. (1998). Noble gases in the Earth’s mantle. *Annu. Rev. Earth Planet. Sci.* 26, 189–218. doi:10.1146/annurev.earth.26.1.189
- Farley, K. A., and Poreda, R. J. (1993). Mantle neon and atmospheric contamination. *Earth Planet. Sci. Lett.* 114, 325–339. doi:10.1016/0012-821X(93)90034-7
- Ferrari, L., López-Martínez, M., Aguirre-Díaz, G., and Carrasco-Núñez, G. (1999). Space-time patterns of cenozoic arc volcanism in central Mexico: From the Sierra Madre Occidental to the Mexican volcanic belt. *Geology* 27, 303–306. doi:10.1130/0091-7613(1999)027<0303:STPOCA>2.3.CO;2
- Ferrari, L., López-Martínez, M., and Rosas-Elguera, J. (2002). Ignimbrite flare-up and deformation in the southern Sierra Madre Occidental, western Mexico: Implications for the late subduction history of the Farallon plate: Ignimbrite flare-up and deformation, western Mexico. *Tectonics* 21, 1–24. doi:10.1029/2001TC001302
- Ferrari, L., Orozco-Esquivel, T., Manea, V., and Manea, M. (2012). The dynamic history of the Trans-Mexican Volcanic Belt and the Mexico subduction zone. *Tectonophysics* 523, 122–149. doi:10.1016/j.tecto.2011.09.018
- Gautheron, C., and Moreira, M. (2002). Helium signature of the subcontinental lithospheric mantle. *Earth Planet. Sci. Lett.* 199, 39–47. doi:10.1016/S0012-821X(02)00563-0
- Gennaro, M. E., Grassa, F., Martelli, M., Renzulli, A., and Rizzo, A. L. (2017). Carbon isotope composition of CO₂-rich inclusions in cumulate-forming mantle minerals from Stromboli volcano (Italy). *J. Volcanol. Geotherm. Res.* 346, 95–103. doi:10.1016/j.jvolgeores.2017.04.001
- Gilfillan, S. M. V., Györe, D., Flude, S., Johnson, G., Bond, C. E., Hicks, N., et al. (2019). Noble gases confirm plume-related mantle degassing beneath Southern Africa. *Nat. Commun.* 10, 5028. doi:10.1038/s41467-019-12944-6
- Goff, F., Janik, C. J., Werner, C., Counce, D., Stímac, J. A., Siebe, C., et al. (1998). Geochemical surveillance of magmatic volatiles at Popocatepetl volcano, Mexico. *GSA Bull.* 110, 695–710. doi:10.1130/0016-7606(1998)110<0695:GSOMVA>2.3.CO;2
- Goff, F., Love, S. P., Warren, R. G., Counce, D., Obenholzner, J., Siebe, C., et al. (2001). Passive infrared remote sensing evidence for large, intermittent CO₂ emissions at Popocatepetl volcano, Mexico. *Chem. Geol.* 177, 133–156. doi:10.1016/S0009-2541(00)00387-9
- Gómez-Tuena, A., Orozco-Esquivel, Ma.T., and Ferrari, L. (2007). “Igneous petrogenesis of the Trans-Mexican volcanic belt,” in *Geology of México: Celebrating the centenary of the geological society of México*. Editors S. A. Alaniz-Álvarez and Á. F. Nieto-Samaniego (Boulder, Colorado: Geological Society of America), 129–181. doi:10.1130/2007.2422(05)
- Graham, D. W. (2002). Noble gas isotope geochemistry of Mid-ocean ridge and ocean island basalts: Characterization of mantle source reservoirs. *Rev. Mineral. Geochem.* 47, 247–317. doi:10.2138/rmg.2002.47.8
- Gurenko, A. A., Hoernle, K. A., Hauff, F., Schmincke, H.-U., Han, D., Miura, Y. N., et al. (2006). Major, trace element and Nd–Sr–Pb–O–He–Ar isotope signatures of shield stage lavas from the central and western Canary Islands: Insights into mantle and crustal processes. *Chem. Geol.* 233, 75–112. doi:10.1016/j.chemgeo.2006.02.016
- Gutmann, J. T. (1986). Origin of four and five-phase ultramafic xenoliths from Sonora, Mexico. *Am. Mineralogist* 71, 1079–1084.
- Halldórsson, S. A., Hilton, D. R., Marshall, E. W., Ranta, E., Ingvason, A., Chakraborty, S., et al. (2022). Evidence from gas-rich ultramafic xenoliths for

- Superplume-derived recycled volatiles in the East African sub-continental mantle. *Chem. Geol.* 589, 120682. doi:10.1016/j.chemgeo.2021.120682
- Harðardóttir, S., Halldórsson, S. A., and Hilton, D. R. (2018). Spatial distribution of helium isotopes in Icelandic geothermal fluids and volcanic materials with implications for location, upwelling and evolution of the Icelandic mantle plume. *Chem. Geol.* 480, 12–27. doi:10.1016/j.chemgeo.2017.05.012
- Heber, V. S., Brooker, R. A., Kelley, S. P., and Wood, B. J. (2007). Crystal–melt partitioning of noble gases (helium, neon, argon, krypton, and xenon) for olivine and clinopyroxene. *Geochim. Cosmochim. Acta* 71, 1041–1061. doi:10.1016/j.gca.2006.11.010
- Henry, C. D., and Aranda-Gomez, J. J. (2000). Plate interactions control middle–late Miocene, proto-Gulf and Basin and Range extension in the southern Basin and Range. *Tectonophysics* 318, 1–26. doi:10.1016/S0040-1951(99)00304-2
- Henry, C. D., and Aranda-Gómez, J. J. (1992). The real southern Basin and Range: Mid- to late Cenozoic extension in Mexico. *Geology* 20, 701–704. doi:10.1130/0091-7613(1992)020<0701:TRSBAR>2.3.CO;2
- Hilton, D., Fischer, T., and Marty, B. (2002). Noble gases and volatile recycling at subduction zones. *Rev. Mineral. Geochem.* 47, 319–370. doi:10.2138/rmg.2002.47.9
- Holland, G., and Ballentine, C. J. (2006). Seawater subduction controls the heavy noble gas composition of the mantle. *Nature* 441, 186–191. doi:10.1038/nature04761
- Hopp, J., Trieloff, M., Buikin, A., Korochantseva, E., Schwarz, W., Althaus, T., et al. (2007a). Heterogeneous mantle argon isotope composition in the subcontinental lithospheric mantle beneath the Red Sea region. *Chem. Geol.* 240, 36–53. doi:10.1016/j.chemgeo.2007.01.004
- Housh, T. B., Aranda-Gómez, J. J., and Luhr, J. F. (2010). Isla Isabel (Nayarit, México): Quaternary alkalic basalts with mantle xenoliths erupted in the mouth of the Gulf of California. *J. Volcanol. Geotherm. Res.* 197, 85–107. doi:10.1016/j.jvolgeores.2009.06.011
- Inguaggiato, S., Martin-Del Pozzo, A. L., Aguayo, A., Capasso, G., and Favara, R. (2005). Isotopic, chemical and dissolved gas constraints on spring water from Popocatepetl volcano (Mexico): Evidence of gas–water interaction between magmatic component and shallow fluids. *J. Volcanol. Geotherm. Res.* 141, 91–108. doi:10.1016/j.jvolgeores.2004.09.006
- Italiano, F., Yuce, G., Di Bella, M., Rojaj, B., Sabatino, G., Tripodo, A., et al. (2017). Noble gases and rock geochemistry of alkaline intraplate volcanics from the Amik and Ceyhan-Osmaniye areas, SE Turkey. *Chem. Geol.* 469, 34–46. doi:10.1016/j.chemgeo.2017.04.003
- IUPAC, 1979. Solubility data series: Helium and neon-gas solubilities. doi:10.18434/T4QC79
- I. Jackson (Editor) (1998). *The Earth's mantle: Composition, structure, and evolution* (Cambridge: Cambridge University Press). doi:10.1017/CBO9780511573101
- Jambon, A., Weber, H. W., and Begemann, F. (1985). Helium and argon from an atlantic MORB glass: Concentration, distribution and isotopic composition. *Earth Planet. Sci. Lett.* 73, 255–268. doi:10.1016/0012-821X(85)90074-3
- Javoy, M., Pineau, F., and Iiyama, I. (1978). Experimental determination of the isotopic fractionation between gaseous CO₂ and carbon dissolved in tholeiitic magma: A preliminary study. *Contr. Mineral. Pet.* 67, 35–39. doi:10.1007/BF00371631
- Kelley, K. A., and Cottrell, E. (2009). Water and the oxidation state of subduction zone magmas. *Science* 325, 605–607. doi:10.1126/science.1174156
- Lages, J., Rizzo, A., Aiuppa, A., Robidoux, P., Aguilar, R., Apaza Choquehuayta, F., et al. (2021b). Crustal controls on light noble gas isotope variability along the Andean Volcanic Arc. *Geochem. Perspect. Lett.* 19, 45–49. doi:10.7185/geochemlet.2134
- Lages, J., Rizzo, A. L., Aiuppa, A., Samaniego, P., Le Pennec, J. L., Ceballos, J. A., et al. (2021a). Noble gas magmatic signature of the Andean Northern Volcanic Zone from fluid inclusions in minerals. *Chem. Geol.* 559, 119966. doi:10.1016/j.chemgeo.2020.119966
- Langmuir, C. H., Vocke, R. D., Hanson, G. N., and Hart, S. R. (1978). A general mixing equation with applications to Icelandic basalts. *Earth Planet. Sci. Lett.* 37, 380–392. doi:10.1016/0012-821X(78)90053-5
- Lee, C. A. (2005). Trace element evidence for hydrous metasomatism at the base of the North American lithosphere and possible association with Laramide low-angle subduction. *J. Geol.* 113, 673–685. doi:10.1086/449327
- Lee, J.-Y., Marti, K., Severinghaus, J. P., Kawamura, K., Yoo, H.-S., Lee, J. B., et al. (2006). A redetermination of the isotopic abundances of atmospheric Ar. *Geochim. Cosmochim. Acta* 70, 4507–4512. doi:10.1016/j.gca.2006.06.1563
- Li, K., Li, L., Pearson, D. G., and Stachel, T. (2019). Diamond isotope compositions indicate altered igneous oceanic crust dominates deep carbon recycling. *Earth Planet. Sci. Lett.* 516, 190–201. doi:10.1016/j.epsl.2019.03.041
- Luhr, J. F., Aranda-Gómez, J. J., and Housh, T. B. (1995a). San Quintín volcanic field, Baja California norte, México: Geology, petrology, and geochemistry. *J. Geophys. Res.* 100, 10353–10380. doi:10.1029/95JB00037
- Luhr, J. F., and Aranda-Gomez, J. J. (1997). Mexican peridotite xenoliths and tectonic terranes: Correlations among vent location, texture, temperature, pressure, and oxygen fugacity. *J. Petrology* 38, 1075–1112. doi:10.1093/ptro/38.8.1075
- Luhr, J. F., Aranda-Gomez, J. J., and Pier, J. G. (1989). Spinel-lherzolite-bearing quaternary volcanic centers in san luis potosí, Mexico: 1. Geology, mineralogy, and petrology. *J. Geophys. Res.* 94, 7916. doi:10.1029/JB094iB06p07916
- Mangler, M., Prytulak, J., Gisbert, G., Delgado-Granados, H., and Petrone, C. M. (2019). Interplinian effusive activity at Popocatepetl volcano, Mexico: New insights into evolution and dynamics of the plumbing system. *Volcanica* 2, 45–72. doi:10.30909/vol.02.01.4572
- Márquez, A., Oyarzun, R., Doblaz, M., and Verma, S. P. (1999a). Alkalic (ocean-island basalt type) and calc-alkalic volcanism in the Mexican volcanic belt: A case for plume-related magmatism and propagating rifting at an active margin? *Geol.* 27, 51–54. doi:10.1130/0091-7613(1999)027<0051:AOIBTA>2.3.CO;2
- Márquez, A., Verma, S. P., Anguita, F., Oyarzun, R., and Brandle, J. L. (1999b). Tectonics and volcanism of Sierra Chichinautzin: Extension at the front of the central Trans-Mexican volcanic belt. *J. Volcanol. Geotherm. Res.* 93, 125–150. doi:10.1016/S0377-0273(99)00085-2
- Martelli, M., Bianchini, G., Beccaluva, L., and Rizzo, A. (2011). Helium and argon isotopic compositions of mantle xenoliths from Tallante and Calatrava, Spain. *J. Volcanol. Geotherm. Res.* 200, 18–26. doi:10.1016/j.jvolgeores.2010.11.015
- Matsumoto, T., Chen, Y., and Matsuda, J.-I. (2001). Concomitant occurrence of primordial and recycled noble gases in the Earth's mantle. *Earth Planet. Sci. Lett.* 185, 35–47. doi:10.1016/S0012-821X(00)00375-7
- Matsumoto, T., Pinti, D. L., Matsuda, J.-I., and Umino, S. (2002). Recycled noble gas and nitrogen in the subcontinental lithospheric mantle: Implications from N-He-Ar in fluid inclusions of SE Australian xenoliths. *Geochem. J.* 36, 209–217. doi:10.2343/geochemj.36.209
- Mattey, D. P. (1991). Carbon dioxide solubility and carbon isotope fractionation in basaltic melt. *Geochim. Cosmochim. Acta* 55, 3467–3473. doi:10.1016/0016-7037(91)90508-3
- McMurtry, G. M., Dasilveira, L. A., Horn, E. L., DeLuze, J. R., and Blessing, J. E. (2019). High ³He/⁴He ratios in lower East Rift Zone steaming vents precede a new phase of Kilauea 2018 eruption by 8 months. *Sci. Rep.* 9, 11860. doi:10.1038/s41598-019-48268-0
- Meriggi, L., MacÀ-as, J. L., Tommasini, S., Capra, L., and Conticelli, S. (2008). Heterogeneous magmas of the quaternary Sierra Chichinautzin volcanic field (central Mexico): The role of an amphibole-bearing mantle and magmatic evolution processes. *Rev. Mex. Cienc. Geol.* 25, 197–216.
- Moreira, M., Kunz, J., and Allègre, C. (1998). Rare gas systematics in popping rock: Isotopic and elemental compositions in the upper mantle. *Science* 279, 1178–1181. doi:10.1126/science.279.5354.1178
- Moreira, M., and Sarda, P. (2000). Noble gas constraints on degassing processes. *Earth Planet. Sci. Lett.* 176, 375–386. doi:10.1016/S0012-821X(00)00010-8
- Mukhopadhyay, S., and Parai, R. (2019). Noble gases: A record of Earth's evolution and mantle dynamics. *Annu. Rev. Earth Planet. Sci.* 47, 389–419. doi:10.1146/annurev-earth-053018-060238
- Németh, K., and Kósik, S. (2020). Review of explosive hydrovolcanism. *Geosciences* 10, 44. doi:10.3390/geosciences10020044
- Nieto-Samaniego, Á. F., Alaniz-Álvarez, S. A., and Camprubí i Cano, A. (2005). La Mesa central de México: Estratigrafía, estructura y evolución tectónica cenozoica. *Bol. Soc. Geol. Mex.* 57, 285–318. doi:10.18268/BSGM2005v57n3a3
- Nieto-Samaniego, Á. F., Ferrari, L., Alaniz-Álvarez, S. A., Labarthe-Hernández, G., and Rosas-Elguera, J. (1999). Variation of Cenozoic extension and volcanism across the southern Sierra Madre Occidental volcanic province, Mexico. *Geol. Soc. Am. Bull.* 111, 347–363. doi:10.1130/0016-7606(1999)111<0347:VOCEAV>2.3.CO;2
- Ozima, M., and Podosek, F. A. (2002). *Noble gas geochemistry*. Cambridge University Press.
- Paonita, A., Caracausi, A., Iacono-Marziano, G., Martelli, M., and Rizzo, A. (2012). Geochemical evidence for mixing between fluids exsolved at different depths in the magmatic system of Mt Etna (Italy). *Geochim. Cosmochim. Acta* 84, 380–394. doi:10.1016/j.gca.2012.01.028

- Paonita, A., and Martelli, M. (2007). A new view of the He–Ar–CO₂ degassing at mid-ocean ridges: Homogeneous composition of magmas from the upper mantle. *Geochim. Cosmochim. Acta* 71, 1747–1763. doi:10.1016/j.gca.2006.12.019
- Parkinson, I. J., and Arculus, R. J. (1999). The redox state of subduction zones: Insights from arc-peridotites. *Chem. Geol.* 160, 409–423. doi:10.1016/S0009-2541(99)00110-2
- Pearson, D. G., Canil, D., and Shirey, S. B. (2014). “Mantle samples included in volcanic rocks,” in *Treatise on geochemistry* (Elsevier), 169–253. doi:10.1016/B978-0-08-095975-7.00216-3
- Peterson, D. B. (1992). *Noble gas geochemistry of selected basalts and andesites: New Zealand, Tonga - kermadec and Vanuatu (PhD)*. Canberra: Australian National University.
- Pier, J. G., Luhr, J. F., Podosek, F. A., and Aranda-Gómez, J. J. (1992). The La breña-el Jagüey maar complex, Durango, Mexico: II. Petrology and geochemistry. *Bull. Volcanol.* 54, 405–428. doi:10.1007/BF00312322
- Pier, J. G., Podosek, F. A., Luhr, J. F., Brannon, J. C., and Aranda-Gómez, J. J. (1989). Spinel-lherzolite-bearing quaternary volcanic centers in san luis potosí, Mexico: 2. SR and ND isotopic systematics. *J. Geophys. Res.* 94, 7941. doi:10.1029/JB094iB06p07941
- Rizzo, A. L., Caracausi, A., Chavagnac, V., Nomikou, P., Polymenakou, P. N., Mandalakis, M., et al. (2019). Geochemistry of CO₂-rich gases venting from submarine volcanism: The case of kolumbo (hellenic volcanic arc, Greece). *Front. Earth Sci.* 7, 60. doi:10.3389/feart.2019.00060
- Rizzo, A. L., Faccini, B., Casetta, F., Faccincani, L., Ntaflos, T., Italiano, F., et al. (2021). Melting and metasomatism in West Eifel and Siebengebirge Sub-Continental Lithospheric Mantle: Evidence from concentrations of volatiles in fluid inclusions and petrology of ultramafic xenoliths. *Chem. Geol.* 581, 120400. doi:10.1016/j.chemgeo.2021.120400
- Rizzo, A. L., Pelorosso, B., Coltorti, M., Ntaflos, T., Bonadiman, C., Matusiak-Malek, M., et al. (2018). Geochemistry of noble gases and CO₂ in fluid inclusions from lithospheric mantle beneath wilcza góra (lower silesia, southwest Poland). *Front. Earth Sci.* 6, 215. doi:10.3389/feart.2018.00215
- Sandoval-Velasquez, A., Rizzo, A. L., Aiuppa, A., Remigi, S., Padrón, E., Pérez, N. M., et al. (2021b). Recycled crustal carbon in the depleted mantle source of El Hierro volcano, Canary Islands. *Lithos* 400–401, 106414. doi:10.1016/j.lithos.2021.106414
- Sandoval-Velasquez, A., Rizzo, A. L., Frezzotti, M. L., Saucedo, R., and Aiuppa, A. (2021a). The composition of fluids stored in the central Mexican lithospheric mantle: Inferences from noble gases and CO₂ in mantle xenoliths. *Chem. Geol.* 576, 120270. doi:10.1016/j.chemgeo.2021.120270
- Sano, Y., and Marty, B. (1995). Origin of carbon in Fumarolic gas from island arcs. *Chem. Geol.* 119, 265–274. doi:10.1016/0009-2541(94)00097-R
- Sano, Y., Nakamura, Y., Wakita, H., Urabe, A., and Tominaga, T. (1984). Helium-3 emission related to volcanic activity. *Science* 224, 150–151. doi:10.1126/science.224.4645.150
- Schaaf, P., Stimac, J., Siebe, C., and Macías, J. L. (2005). Geochemical evidence for mantle origin and crustal processes in volcanic rocks from Popocatepetl and surrounding monogenetic volcanoes, Central Mexico. *J. Pet.* 46, 1243–1282. doi:10.1093/petrology/egi015
- Sedlock, R. L. (2003). “Geology and tectonics of the Baja California Peninsula and adjacent areas,” in *Tectonic evolution of northwestern Mexico and the southwestern USA* (Boulder, Colorado: Geological Society of America). doi:10.1130/0-8137-2374-4.1
- Sedlock, R. L., Ortega-Gutiérrez, F., and Speed, R. C. (1993). *Tectonostratigraphic terranes and tectonic evolution of Mexico*. Boulder, Colorado: Geological Society of America Special Papers Geological Society of America. doi:10.1130/SPE278
- Severinghaus, J., and Atwater, T. (1990). “Chapter 1: Cenozoic geometry and thermal state of the subducting slabs beneath western North America,” in *Geological society of America memoirs* (Boulder, Colorado: Geological Society of America), 1–22. doi:10.1130/MEM176-p1
- Straub, S., Batanova, V. G., Gómez-Tuena, A., Espinasa-Perena, R., Fleming, W. L., Bindeman, I. N., et al. (2022). Olivine Ca as proxy to mantle wedge depletion in the Trans-Mexican volcanic belt.
- Straub, S. M., Gómez-Tuena, A., Bindeman, I. N., Bolge, L. L., Brandl, P. A., Espinasa-Perena, R., et al. (2015). Crustal recycling by subduction erosion in the central Mexican Volcanic Belt. *Geochim. Cosmochim. Acta* 166, 29–52. doi:10.1016/j.gca.2015.06.001
- Straub, S. M., Gomez-Tuena, A., Stuart, F. M., Zellmer, G. F., Espinasa-Perena, R., Cai, Y., et al. (2011). Formation of hybrid arc andesites beneath thick continental crust. *Earth Planet. Sci. Lett.* 303, 337–347. doi:10.1016/j.epsl.2011.01.013
- Straub, S. M., Gómez-Tuena, A., Zellmer, G. F., Espinasa-Perena, R., Stuart, F. M., Cai, Y., et al. (2013). The processes of melt differentiation in arc volcanic rocks: Insights from OIB-type Arc magmas in the central Mexican volcanic belt. *J. Pet.* 54, 665–701. doi:10.1093/petrology/egs081
- Straub, S. M., LaGatta, A. B., Martin-Del Pozzo, A. L., and Langmuir, C. H. (2008). Evidence from high-Ni olivines for a hybridized peridotite/pyroxenite source for orogenic andesites from the central Mexican volcanic belt: Andesite petrogenesis in central mxb. *Geochim. Geophys. Res.* 9, na. doi:10.1029/2007gc001583
- Straub, S. M., Zellmer, G. F., Gómez-Tuena, A., Espinasa-Pereña, R., Martin-del Pozzo, A. L., Stuart, F. M., et al. (2014). A genetic link between silicic slab components and calc-alkaline arc volcanism in central Mexico. *Geol. Soc. Lond. Spec. Publ.* 385, 31–64. doi:10.1144/SP385.14
- Swanson, E. R. (1989). *A new type of maar volcano from the State of Durango-the El Jagüey-La Breña complex reinterpreted*, 8. Ciudad de México: Universidad Nacional Autónoma de México, Revista del Instituto de Geología, 243–248.
- Taran, Y., Inguaggiato, S., Varley, N., Capasso, G., and Favara, R. (2002). Helium and carbon isotopes in thermal waters of the Jalisco block, Mexico. *Geofísica Int.* 41.
- Trull, T. W., and Kurz, M. D. (1993). Experimental measurements of ³He and ⁴He mobility in olivine and clinopyroxene at magmatic temperatures. *Geochim. Cosmochim. Acta* 57, 1313–1324. doi:10.1016/0016-7037(93)90068-8
- Urrutia-Fucugauchi, J., and Böhnel, H. (1988). Tectonics along the Trans-Mexican volcanic belt according to palaeomagnetic data. *Phys. Earth Planet. Interiors* 52, 320–329. doi:10.1016/0031-9201(88)90124-0
- Urrutia-Fucugauchi, J., Flores-Ruiz, J. H., Bandy, W. L., and Mortera-Gutiérrez, C. A. (1999). Crustal structure of the Colima rift, western Mexico: Gravity models revisited. *Geofit.* 38, 205–216. doi:10.22201/igeof.00167169p.1999.38.4.503
- Vance, D., Stone, J. O. H., and O’Nions, R. K. (1989). He, Sr and Nd isotopes in xenoliths from Hawaii and other oceanic islands. *Earth Planet. Sci. Lett.* 96, 147–160. doi:10.1016/0012-821X(89)90129-5
- Williams, S. N., Sano, Y., and Wakita, H. (1987). Helium-3 emission from Nevado del ruiz volcano, Colombia. *Geophys. Res. Lett.* 14, 1035–1038. doi:10.1029/GL014i010p01035
- Witter, J. B., Kress, V. C., and Newhall, C. G. (2005). Volcán Popocatepetl, Mexico. Petrology, magma mixing, and immediate sources of volatiles for the 1994–present eruption. *J. Pet.* 46, 2337–2366. doi:10.1093/petrology/egi058
- Wood, B. J., Bryndzia, L. T., and Johnson, K. E. (1990). Mantle oxidation state and its relationship to tectonic environment and fluid speciation. *Science* 248, 337–345. doi:10.1126/science.248.4953.337
- Yamamoto, J., Nishimura, K., Sugimoto, T., Takemura, K., Takahata, N., and Sano, Y. (2009). Diffusive fractionation of noble gases in mantle with magma channels: Origin of low He/Ar in mantle-derived rocks. *Earth Planet. Sci. Lett.* 280, 167–174. doi:10.1016/j.epsl.2009.01.029